Low-temperature spectroscopic studies of single molecules in 3-D and on 2-D hosts

Smit, R.

5

HEXAGONAL BORON NITRIDE: A UNIVERSAL HOST MATRIX?

In this chapter, I will present the studies that we performed on an unconventional host for single molecules, namely two-dimensional hexagonal boron nitride (hBN). We will show that single molecules on the surface of hBN reveal narrow spectral lines at low temperature. Contrary to molecules on surfaces of three-dimensional (organic) crystals, we were able to record excitation spectra of the molecule's zero-phonon lines on the surface of hBN and reveal linewidths that are sometimes less than a factor 10 broader than the lifetime-limited linewidth, as dictated by the fluorescence lifetime. This new host could potentially overcome the limitations of three-dimensional organic matrices, which require a 'good' insertion of the guest molecules. However, molecules on hBN are subject to a spectral diffusion and this currently limits the usability of this system for applications such as sensing at the nanoscale or uses in quantum optics. We will show that thermal annealing of the hBN, before deposition of the molecules, dramatically improves the stability of the molecules and this indicates it might be possible to eliminate spectral diffusion altogether. In this study, we will focus on terrylene molecules adsorbed onto hBN. In addition, we will show some results of new types of molecules, called graphene quantum dots, which have not been studied before in line-narrowing spectroscopy. Due to their bulkiness, these type of molecules are difficult to incorporate in standard host matrices and therefore these studies underline the potential to extend the use of hBN to a large variety of guest molecules.

Part of the contents of this chapter is published as: R. Smit, A. Tebyani, J. Hameury, S.J. van der Molen and M. Orrit, "Sharp zero-phonon lines of single organic molecules on a hexagonal boron-nitride surface", Nature Communications 14, 7960 (2023)

5.1. INTRODUCTION

5.1.1. HEXAGONAL BORON NITRIDE

Similar to graphene, hexagonal boron-nitride (hBN) is a two-dimensional material that possesses a hexagonal lattice (Figure 5.1). However, unlike graphene, the alternating arrangement of boron and nitrogen opens up a large electronic band gap of about 6 eV,[1] which makes it optically transparent. hBN is therefore usually termed 'white graphene'. Importantly, the large band gap of hBN avoids what would happen with fluorescent molecules in contact with graphene or other small bandgap materials, namely fluorescence quenching by non-radiative energy transfer.[2] The similar structure, bond lengths and the van der Waals interactions that exist in multilayer hBN, make hBN an interesting host material for polycyclic aromatic hydrocarbons, which are interacting through van der Waals forces among each other as well. Fluorescent terrylene molecules, deposited on hBN, were already measured at room temperature by Han *et al*.[3] Interestingly, this work suggests that the terrylene molecules are protected by the hBN, as bleaching rates of single molecules were more than a hundred-fold reduced on hBN, as compared to single molecules on bare silica.

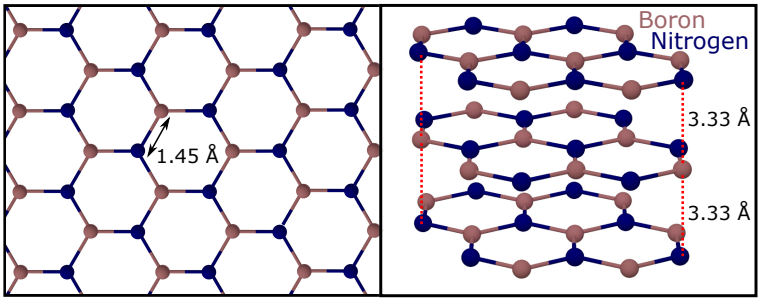

Figure 5.1.: Structure of hexagonal boron-nitride. Boron and nitrogen are alternatingly arranged, with an interatomic distance of 1.45 Å. In multilayer hBN, the layers stack such that a nitrogen atom faces a boron atom and vice versa. The interlayer distance is 3.33 Å, which is the same as for graphene.[4]

As a model molecule for our studies of hBN, we also employed terrylene. No further introduction of this molecule is required, as it is already part of an extensive study in Chapter 4. hBN can be synthesized in several forms, such as free-standing crystals or grown onto a substrate. On a substrate, such as Cu(111), wafer-scale monolayers of hBN can be grown by chemical vapor deposition.[5] Free-standing crystals of hBN are traditionally grown by chemical reactions at high temperature and high pressure.[6] This is also the method used by T. Taniguchi and K. Watanabe from NIMS,[7] whose hBN crystals are regarded to be of the best quality. Since the first discovery of single-photon emitters in hBN,[8] a new and nowadays rich field of research has emerged. Since then, many types of distinct emitters in hBN, typically attributed to light-emitting defects, have been reported. The fluorescence from these emitters peaks over a surprisingly broad spectral range, from the deep ultraviolet[9] up to the near-infrared,[10] with many more at

in-between wavelengths. The atomic and electronic structure of the claimed defects still remains a puzzle and only educated guesses as to their origin have been made from quantum-chemistry models.[11–14] Since the start of our work, new perspectives on some of these emitters have arisen, such as that some of their origins could be traced back to organic compounds formed during preparation steps that involves high-temperature thermal annealing.[15]

5.1.2. LOW-TEMPERATURE SPECTROSCOPY ON SURFACES

At room temperature, the surface of a substrate is commonly used to study single molecules. At low temperature, on the contrary, surfaces are not a stable environment compared to the bulk of a solid. Early studies of single molecules in a hexadecane crystal revealed that molecules closer to the interface with silica had strongly broadened zero-phonon lines, while no zero-phonon line was detected for single molecules at the silica surface itself.[16] Later experiments on dibenzanthanthrene (DBATT) inside nanochannels filled with matrices of naphthalene and n-tetradecane confirmed that molecular spectral lines were broader when the channel decreased in height and molecules would be located closer to the interfaces.[17] Lastly, the study of fluorescent molecules evaporated onto a polymer layer, controllably heated to allow the molecules to diffuse into the polymer and settle at controllable mean depths, showed likewise that molecules closer to the surface exhibited strongly broadened zero-phonon lines. Interestingly, the amount of spectral diffusion was also significantly higher for molecules closer to the surface and no zero-phonon line could be detected closer than 0.5 nm to the surface.[18] Beyond single-molecule studies, narrow ZPLs down to 500 MHz in width have been observed through hole-burning spectroscopy, e.g. for chemisorbed, and thus strongly bound, quinizarin on alumina surfaces,[19] but this particular method relies on weak photostability and thus renders it impossible to detect single molecules.

The causes for the anomalous behavior of ZPLs of single molecules close to a surface or interface as compared to molecules in the bulk is still under debate. Possibly, high densities of two-level systems (TLSs) at or close to the surface have lower activation energies due to the ill-condensed boundaries of a crystal. Impurities could also pile up at the crystal boundaries due to expulsion from the bulk or by adsorption from the environment and give rise to a local increase of conformational states. Despite these surface-induced effects on ZPLs, it has been possible to reduce the dimensions of host-guest crystals and yet obtain near-lifetime-limited emission in the bulk of aromatic nanocrystals less than 100 nm thick, grown by reprecipitation from solution.[20,21] Thinner matrices for single molecules are highly desirable for applications such as single-charge sensing, which requires a close proximity of the sensing molecules to the charge,[22] or potential applications in nanophotonics. For the latter case, such systems-on-a-chip make use of dielectric waveguides, and a closer proximity of single molecules to waveguides is expected to lead to a better coupling to the evanescent field. The coupling of single molecules to waveguides on a chip was demonstrated in 2017.[23] Later experiments with waveguide-coupled single dibenzoterrylene (DBT) molecules revealed spectral diffusion of the 0-0 ZPL under an applied electric field, attributed to charge fluctuations induced within the nanoguide itself.[24] With high-quality anthracene crystals of about 150 nm

in thickness, suspended over the waveguide channels, it was demonstrated that DBT molecules coupling to the waveguide remain stable and near-lifetime-limited for hours.[25]

5.2. EXPERIMENTAL

5.2.1. SAMPLE PREPARATION

In most experiments, we made use of free-standing crystals, purchased from the company HQ Graphene. In the remaining experiments (to be mentioned in the text) we employed high-quality crystals from NIMS, with permission shared with us by dr. Semonti Bhattacharyya from Leiden University. The crystals of both sources are typically up to a few mm large and multilayered. To obtain flakes of hBN on a substrate we use the commonly-employed method of exfoliation using scotch tape, which was established by A. Geim and K. Novoselov to obtain graphene monolayers.[26] The repeated use of the scotch tape cleaves the thick crystals into thinner (and smaller) crystals, which can be transferred to a substrate. The tape is stuck to the substrate and heated to 120 ˚C for 2 minutes on a hot plate to improve the adhesion of the flakes to the substrate. Then the tape is removed, while some flakes stay behind (Figure 5.2). As a typical substrate we used a Si wafer with a thermally-grown oxide layer of 300 nm, bought from University Wafer. Before deposition of hBN, the substrate was typically cleaned with acetone.

Molecules were either diluted in toluene (Acros Organics, 99.85 %) and spin-coated on the substrates or directly sublimated from crystals. For the preparation by spin coating, the concentration of molecules in toluene was diluted to 0.1-1 nM and about 30-50 μL of the solution was pipetted on the substrate and spin coated for 20 s at 2000 rpm, followed by a drying step at 4000 rpm for another 20 s. For sublimation, pure crystals of terrylene were placed at the bottom of a vacuum sublimation apparatus, where the substrate was suspended on a cold finger, cooled by water ice (Figure 5.3). The atmosphere was pumped to vacuum and the bottom was heated to 120-140 ˚C, in order to obtain a similar concentration as obtained through spin coating.

For the fluorescence measurements we used the setup as described in Chapter 2 in Figure 2.3. In the early experiments, the flakes were used immediately, but later we performed post-processing on the flakes, such as thermal annealing. Thermal annealing was performed in a Thermcraft tube oven in a moderate vacuum of about 10^{-2} mbar of residual air. The annealing temperatures were varied between 500–900 ˚C with a dwell time of up to 12 hours. Height profiles of the hBN flakes were measured by AFM.

5.3. RESULTS AND DISCUSSION

5.3.1. PROPERTIES OF THE HBN FLAKES

Atomic force microscopy (AFM) measurements show that most of the hBN flakes have a thickness of less than 100 nm (about 300 layers), with some exceptions of thick flakes of a few 100 nm. The AFM scans in Figure 5.4 show flakes that were either annealed or not annealed. On the flakes themselves, there is no noticeable difference in the AFM scans between Figure 5.4e and Figure 5.4f, which is measured before and after annealing. In the regions outside of the flakes, the residue from the scotch tape (mostly

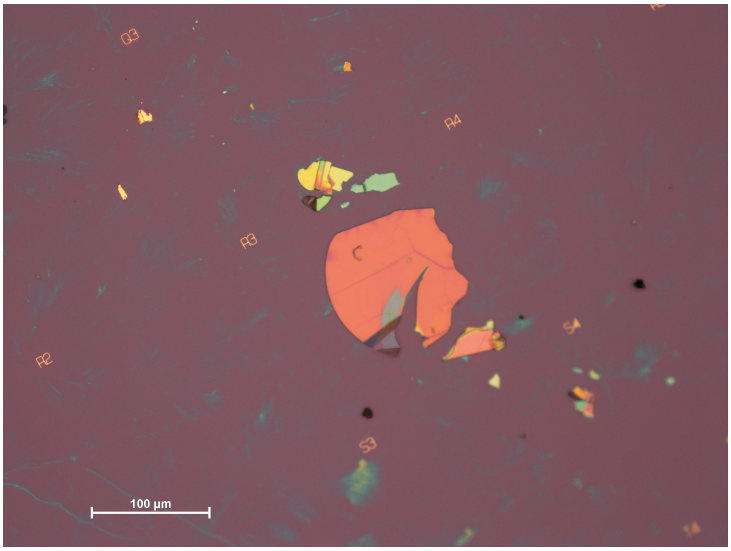

Figure 5.2.: . Microscope image of a collection of hBN flakes that are obtained by exfoliation. The sizes of the flakes vary from sub-µm to large flakes of up to a few 100 µm. The color of the flakes gives a rough indication of the thickness, as it arises from interference of light reflected from the interfaces.[27] Typically, the bluish flakes are the thinnest, while reddish flakes are the thickest. The blue-green-yellowish clouds in the background are polymer residues from the scotch tape.

polymers) is removed efficiently by thermal annealing. However, the surface roughness on the flakes themselves is preserved, as the contamination could be located under the flake and is therefore protected.

As part of surface roughness, there are sometimes bubbles present in the AFM scans (see for example one in the left corner of Figure 5.4e). These bubbles or pockets are likely due to pile-up of organic contamination between the hBN sheets or at the interface, and were similarly observed in heterostructures of 2D materials by cross-sectional imaging.[28] Step edges, due to a decrease or increase in layer count, also occur in the scans, but are sometimes difficult to see, because of their low contrast. Such step edges are better visualized on extended terraces, present as sharp lines in Figure 5.5. Other anomalies are the sharp increases in height, such as found in Figure 5.4d. These are likely caused by wrinkles in the sheet, where the layers fold up. The formation of wrinkles was found to be enhanced by annealing at similar temperatures as we used.[29] On the extended terraces, the surface can be almost atomically flat as shown in Figure 5.5, where the surface height deviations reach 0.41 nm, close to the interlayer distance of 0.33 nm. Although this could indicate a small variation in layer count, the measured values are likely limited by the AFM resolution and the surface roughness of the wafer substrate.

The lattice of hBN has only one weakly active Raman mode around 1,365 cm^{-1},

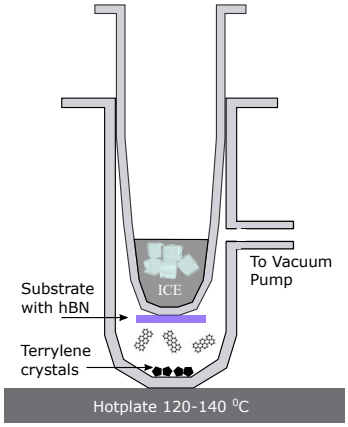

Figure 5.3.: Schematic representation of the sublimation apparatus, which consists of two round-bottom flasks, where the top one is inserted into the bottom one, sealed by vacuum grease (Apiezon) and pumped by a vacuum pump from the side. The bottom of the flask is heated on a hot plate to approximately 120-140 °C. The crystals are placed inside, in contact with the heated bottom. The sample is fixed with carbon tape on the cold finger and cooled by water ice.

attributed to the stretching of the bond between boron and nitrogen. We observed this Raman peak with a relatively strong 532 nm laser spot, shown in Figure 5.6. The width of the Raman peak of about 10 cm^{-1} depends not only on crystal quality, but also on the isotopic distribution. In high-quality crystals grown with natural abundances of isotopes, ^{14}N and ^{15}N for nitrogen and ^{10}B and ^{11}B for boron, the Raman peak has a minimum width of about 7.3-7.5 cm^{-1}.[30] Hence, the 10 ± 1 cm^{-1} measured in our samples may be the result of a poorer crystallinity, although the measured linewidth conforms to the report of HQ Graphene. For the hBN from NIMS, regarded to be of higher quality, the Raman peak measured the same width within the uncertainty.

5.3.2. ROOM-TEMPERATURE FLUORESCENCE MEASUREMENTS

After deposition of molecules on the hBN substrate, we measured the spatial distribution of the emitters and their spectra at room temperature. In the case of sublimated molecules on non-annealed hBN flakes, we find molecules to be located everywhere on the hBN flake (see Figure 5.7a). However, some regions tend to be more packed with molecules than others are. For example, the sharp edge in Figure 5.7a, possibly a step edge or wrinkle, contains a lot more fluorophores than the stretched and presumably flat regions. Interestingly, this packing of emitters was similarly observed for defect emitters, which are in exfoliated hBN also preferentially located around sharp edges.[31,32] However, both reports concern emitters that were activated by

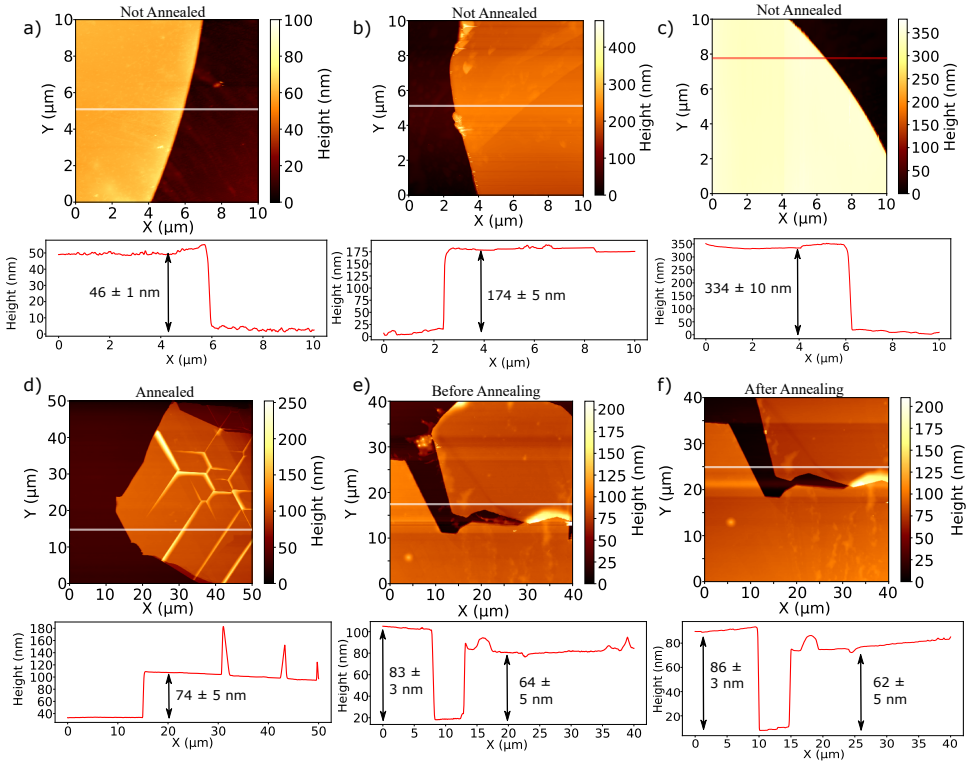

Figure 5.4.: a,b,c) AFM scans of a small part (10x10 μm^2) of non-annealed exfoliated hBN flakes on a Si/SiO_2 substrate with below each 2D map the corresponding height profile, recorded along the white line (red for (c)). The flake in (d) is annealed at 500 ˚C for 12 hours. The AFM images in (e) and (f) show the same flake, respectively before and after annealing at 500 ˚C for 12 hours.

thermal annealing, which as mentioned before could create organic molecule emitters.[15] Furthermore, our molecules have found some place to immobilize, as was already observed by Han *et al*., and can be measured up to a few minutes of time until bleaching occurs. In samples with a very high concentration of terrylene, the bleaching is clearly observed as a single exponential decay in the measured fluorescence signal, where the time constant is typically in the order of minutes (Figure 5.7b). This bleaching rate is relatively fast and may indicate that most (sublimated) molecules are not so well protected by the hBN, as suggested for the spin-coated molecules by Han *et al*. For spin-coated molecules it might be possible that some molecules diffuse from the solvent between the interface of silica and hBN.[33]

The room-temperature spectra of the fluorescence emission from the isolated spots

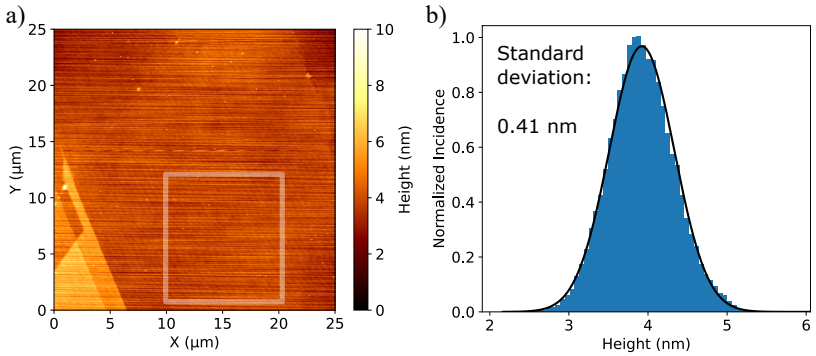

Figure 5.5.: AFM scan of a flat area of an annealed hBN flake (500 ˚C for 12 hours). The white rectangle encloses the region that builds up the histogram in b). The Gaussian distribution of surface heights shows a standard deviation of 0.41 nm. Tilts and drifts in the scan have been subtracted by a line-by-line linear fit.

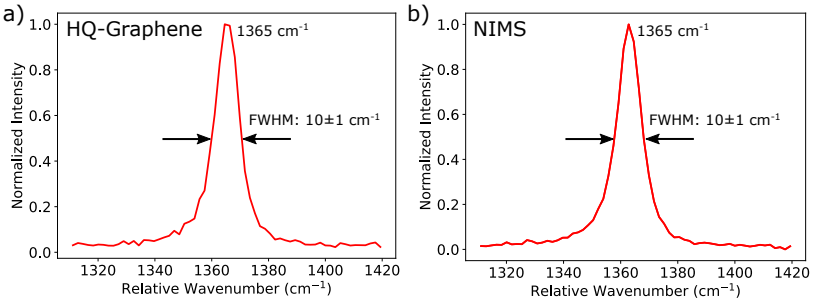

Figure 5.6.: Spectra of the inelastically-scattered light from a multilayer hBN flake (from supplier HQ Graphene in panel (a) and NIMS in panel (b)), taken with a 532 nm laser. The single Raman peak observed for both cases at 1365 cm^{-1}, with a FWHM of 10 ± 1 cm^{-1}, was taken at a resolution of around 1-2 cm^{-1}. The spectrum is recorded at room temperature with a 1200 lines/mm grating and a 0.1 mm slit size.

displays a shape that conforms to the emission spectrum of terrylene, but also of many other polycyclic aromatic hydrocarbons (PAHs). The spectra are heavily broadened at room temperature and few features can be resolved, apart from the large spectral bands around the 0-0 zero-phonon line, the C-C stretch region and overtones (Figure 5.8a). All of them are also present for other PAHs. However, for some isolated emitters, the spectra did reveal more features, such as in Figure 5.8b. The positions of these bands coincide with the well-resolved spectral lines that we recorded at low temperature, which will be shown in the next section.

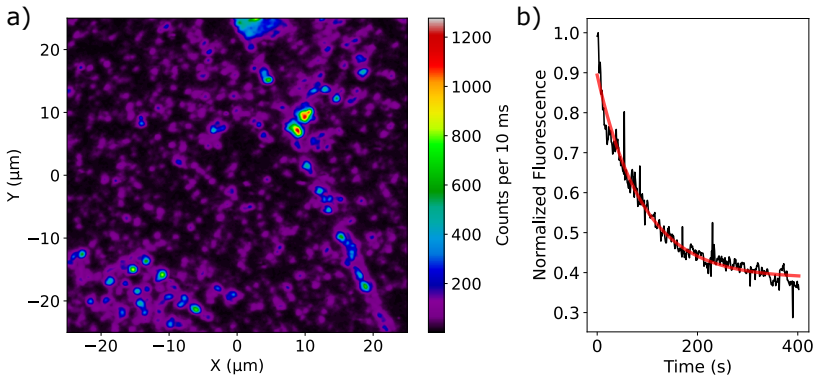

Figure 5.7.: Panel (a) shows a fluorescence map of a part of an hBN flake. The terrylene molecules are sublimated, using the setup in Figure 3, at 120 ˚C for 5 minutes and excited by a vibronic transition with 532 nm light. The faintest and most isolated spots of purplish color are possibly single molecules (antibunching measurements were only made at low temperature, in absence of photobleaching), while brighter spots are likely multiple molecules in the same focal area. The image was recorded at an excitation intensity of about 10 kW/cm^2. At similar power levels, and high concentration of terrylene, bleaching occurs at room temperature at timescales in the order of minutes, as shown in panel (b). The characteristic time of the single exponential decay is here around 90 s. The data is measured from the integrated intensity of emission spectra. Deviations due to cosmic rays in the spectra, which are not filtered, are probably the cause of the peaks. Note that the bleaching does not extend to zero and may be caused by some population of molecules that bleach on a much longer timescale and/or contributions from molecules further away from the peak of the diffraction-limited laser spot.

Surprisingly, a major discrepancy exists between the spectra in Figure 5.8 and the results of Han *et al*. The emission intensity peaks around 580 nm, while Han *et al*. reported an emission peak around 600 nm. This is a significant red-shift of the emission peak, which is not regularly observed for terrylene in organic matrices. Only for terrylene in *p*-dichlorobenzene,[34] with a site around 597 nm, and terrylene in BTBT at 602 nm (see Figure 4.1 in Chapter 4), the emission is shifted that far to the red. Although the majority of terrylene molecules do display an emission around 580 nm in our work, we will show that after annealing of the hBN flakes, a population of molecules around 600 nm does appear in the inhomogeneous broadening.

5.3.3. LOW-TEMPERATURE SPECTRA OF TERRYLENE ON HBN

By cooling down our hBN samples covered with terrylene, we observe a strong line narrowing of the emission spectra. This allows us to identify each emitter located on

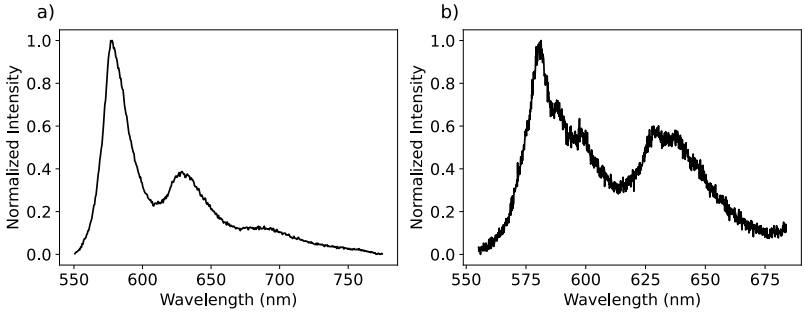

Figure 5.8.: Fluorescence emission spectra of terrylene at room temperature. The spectrum in (a) is likely from an ensemble of terrylene molecules, while the spectrum in (b) might be from a single molecule, as the emission was relatively isolated.

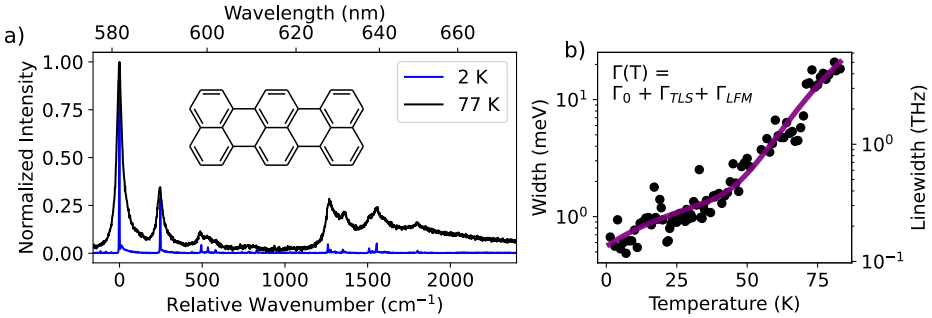

Figure 5.9.: Emission spectra of a single terrylene molecule around 582 nm, taken at two temperatures, 2 K (blue) and 77 K (black). Both spectra have been normalized to unity relative to the intensity of the 0-0 ZPL. b) Linewidth of the 0-0 ZPL of a single terrylene molecule (not the one shown in (a)). The linewidth was fitted to the equation in inset, where Γ_{TLS} scales linearly with temperature and Γ_{LFM} is given by the Arrhenius law, described in equation 5.1. The linewidth at the lowest temperature was limited by the spectrometer resolution (1.7 ± 0.1 cm^{-1}). A zoomed-in version of the spectrum in (a) can be found in Figure 5.11b.

the hBN flake by its vibrational fingerprint. The blue curve in Figure 5.9a shows sharp spectral lines, limited in width by the spectrometer resolution of about 1.7 ± 0.1 cm^{-1}. Even at liquid-nitrogen temperatures of 77 K, the coarse spectral fingerprint of the emitter could be resolved with relative ease, which makes the use of liquid helium not necessary for identification of the emitters. The sharpest line in the spectrum is the 0-0 ZPL and corresponds to the purely electronic transition. The remaining peaks correspond

to a transition that involves an additional excitation of a (or multiple) vibration(s). These vibrational energies have been analyzed for terrylene in great detail in various matrices[35–37] and can also be found in the spectrum of terrylene in BTBT, Figure 4.1 in chapter 4. The line narrowing of the 0-0 ZPL follows the relationship with temperature shown in Figure 5.9b. Here, we measured the linewidth or full-width-at-half-maximum for 88 intermediate temperatures over the range of 1.4 K up to 83 K. The 0-0 ZPL linewidth follows the broadening relation that is consistent with defects in hBN[38,39] or disordered matrices, such as polymers:[40]

$$\Gamma(T) = \Gamma_0 + \Gamma_{TLS} + \Gamma_{LFM} = \Gamma_0 + bT^{\alpha} + w \times \exp\left(-E_a/k_B T\right). \tag{5.1}$$

The first term Γ_0 is the homogeneous linewidth, while the broadening terms Γ_{TLS} and Γ_{LFM} account for respectively the activation of switching two-level systems (TLSs) and the population of quasi-localized low-frequency modes (LFMs). In general, two-level systems are activated in a linear fashion with temperature, with $\alpha \approx 1$. The LFMs are activated by an Arrhenius law and provide an activation energy or Debye temperature of the molecule in its insertion site. Comparing the broadening of terrylene on hBN to traditional three-dimensional matrices we find in the limited amount of works available that the linewidth at 50 K of about 25 cm^{-1} is very similar to the linewidth of terrylene found in the Shpol'skii matrices n-hexadecane and n-dodecane,[41] with respectively 33 ± 3 cm^{-1} and 21 ± 3 cm^{-1}. However, the contribution from TLSs, which we estimate as 5 ± 3.5 GHz/K (21 ± 14 μeV/K) seems to be considerably larger than the typically less than 100 MHz/K found in Shpol'skii matrices.[40] The similar linewidth of terrylene on hBN compared to a Shpol'skii matrix and the higher TLS broadening on hBN could mean that molecules in Shpol'skii systems broaden quicker at lower temperatures. As we will show later, the TLSs are likely attributed to organic contamination on the surface of hBN and thus the closer proximity of these TLSs might be responsible for the stronger broadening. Beyond this linear regime of TLSs, there is a clear exponential take-off from about 50 K, which corresponds to a rather high activation energy or Debye temperature of 405 ± 41 K. This is considerably higher than the regular 10-40 K observed for example in the case of dibenzoterrylene (DBT) in anthracene[42–44] and found in all organic matrices. However, DBT molecules in anthracene broaden with a pure Arrhenius curve and do not suffer from additional broadening of the homogeneous linewidth due to TLSs.

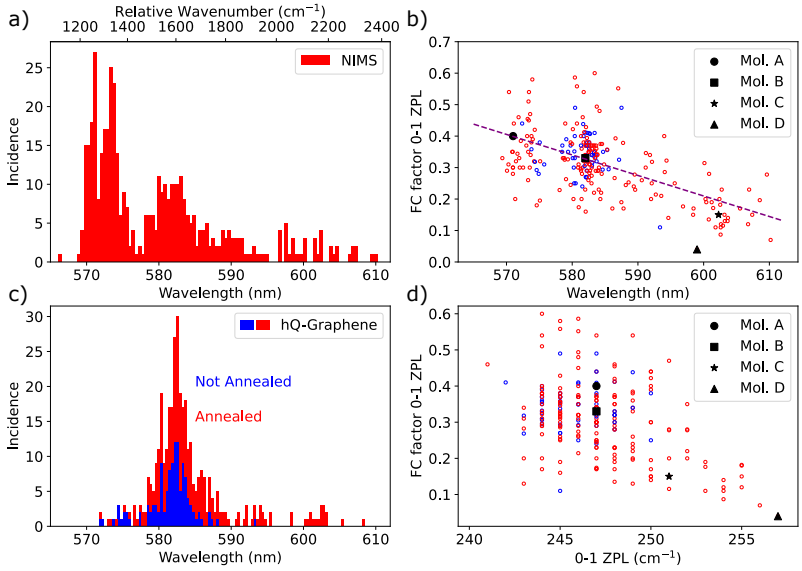

Figure 5.10.: Panel (a) displays the histogram of wavelengths where we found the purely-electronic transition of single terrylene molecules on hBN flakes from NIMS. All data was recorded with a fixed 532 nm excitation laser and for reference the relative difference in energy between this laser and the 0-0 ZPL of the molecules is shown on the top axis in wavenumbers. Note that some structure is present in the histogram, which might arise from absorption peaks that reflect the vibrational spectra in Figure 5.11 of terrylene. Hence, some molecules may not appear in the histogram, because there are no absorption lines present at 532 nm. This suggests that there might be a continuous distribution, spanning a large range of more than 40 nm. All data of 452 individual molecules is obtained from annealed hBN. Panel (b) shows for 237 molecules (58 molecules for non-annealed hBN in blue color), both from hBN from NIMS and HQ Graphene, the relation between the relative intensity of the main vibration (0-1 ZPL) versus the position of the 0-0 ZPL. On average, the more red-shifted molecules have a weaker vibronic coupling (Pearson's correlation coefficient r = -0.56). In panel (c) a similar distribution is shown as for (a), but for hBN from the supplier HQ Graphene and taken from both annealed (red data) and non-annealed (blue) hBN. The total number of molecules in the histogram amounts to 373 (123 for non-annealed and 250 for annealed hBN). Panel (d) shows the relation between the energy of the 0-1 ZPL and the relative intensity of the 0-1 ZPL compared to the 0-0 ZPL. Overall, a decrease in the Franck-Condon (FC) factor of the 0-1 ZPL is measured when the energy of the 0-1 ZPL is higher. The symbols displayed in panel (b) and panel (d) refer to the molecules that are plotted in Figure 5.11.

We find the 0-0 ZPLs of terrylene molecules to be scattered over a broad range, though with clustering around specific wavelengths (see Figure 5.10a and 5.10c). We started initial experiments with hBN obtained from HQ Graphene and the inhomogeneous broadening of terrylene on flakes of that particular manufacturer centers mostly around 582 nm. This distribution, found in Figure 5.10c, is relatively broad with a width of about 4 nm (120 cm^{-1}), which is compared to other hosts only typical for disordered systems such as polyethylene.[45] For the case of hBN obtained from NIMS, we measure a very different distribution of 0-0 ZPLs, which rather looks like a signature of a larger continuous distribution, spanning over 40 nm. This continuous distribution displays gaps and a structure that reminds of the vibrational spectrum of terrylene, where the structure is given by the energy difference between the 532 nm laser and the 0-0 ZPL position; a narrow absorption spectrum. This could indicate that we are not seeing all molecules with our fixed-frequency laser, as those molecules could simply lack absorption lines in resonance with the laser. Surprisingly, the inhomogeneous broadening of terrylene on NIMS hBN peaks around 572 nm instead of 582 nm. This marked difference still remains to be explained.

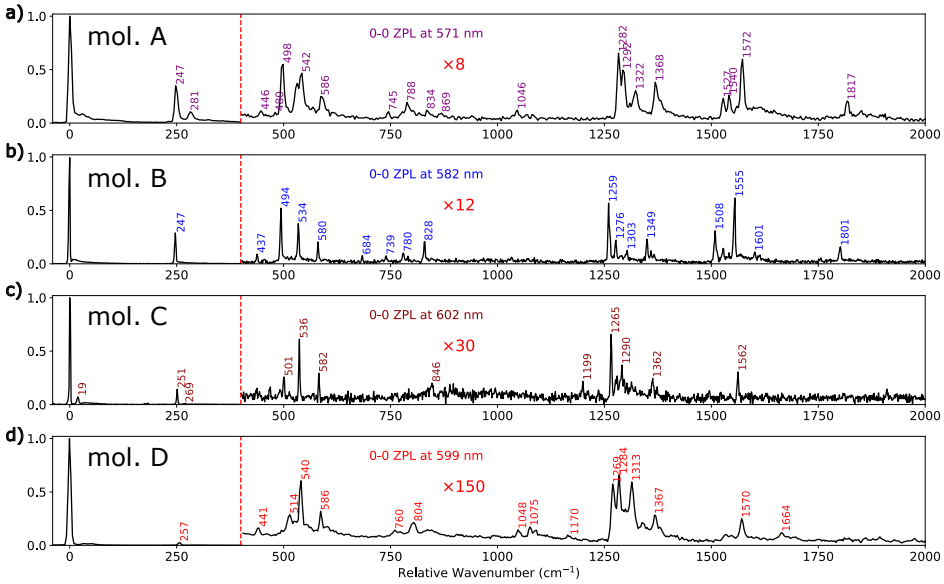

Figure 5.11.: Comparison of fluorescence emission spectra of single terrylene molecules at various positions in the inhomogeneous broadening. The spectrum in panel (a) is from a molecule with a 0-0 ZPL at 571 nm, taken on annealed hBN from NIMS. Panel (b) shows the detailed spectrum of the molecule in Figure 5.9a (blue curve), with a 0-0 ZPL at 582 nm and taken on HQ Graphene hBN (not annealed). Panel (c) shows a red-shifted molecule (602 nm) taken on HQ Graphene hBN that was annealed. Another red-shifted molecule at 599 nm is shown in panel (d), taken on annealed NIMS hBN. Note that the red-shifted molecules have weaker Franck-Condon factors, where in the extreme case of molecule D, the part of the spectrum after 400 cm^{-1} is magnified by 150x for comparison. Moreover, the phonon sidebands are weaker for the red-shifted molecules. In the case of (d), the Debye-Waller factor ($=I_{ZPL}/(I_{ZPL}+I_{PSB})$) is more than 0.9. The spectra in (a) and (d) were taken with a slightly lower resolution of 600 lines/mm at a 0.1 mm slit size of the spectrometer in order to capture the whole spectrum at once. The spectra in (b) and (c) were taken with the higher resolution grating of 1200 lines/mm and 0.1 mm slit size and are therefore stitched by two individual recordings.

On hBN flakes that were annealed prior to molecule deposition, as compared to non-annealed flakes, we find molecules with considerably red-shifted 0-0 ZPLs. Surprisingly, the red-shifted molecules show a reduced vibronic coupling (Franck-Condon factors) between the excited state and vibronic levels of the ground state. Overall, we observe a decrease of the Franck-Condon (FC) factors when the 0-0 ZPL shifts to the red, as observed in Figure 5.10b, where examples of emission spectra in various positions

along the inhomogeneous broadening are additionally shown in Figure 5.11. Moreover, there appears to be a weak relation between the 0-0 ZPL position and the energy of the main vibration (frequency difference between the 0-1 ZPL and the 0-0 ZPL), shown in Figure 5.10c. In extreme cases, the FC factors show a suppression to such an extent that the bulk of emission is directed into the 0-0 ZPL. This can be expressed in a quantity that is called the branching ratio ($= I_{ZPL}/I_{spectrum}$) and amounts to the molecule in Figure 5.11d to at least 78%. This feature is particularly interesting for the generation of indistinguishable photons in quantum optics. In view of this application, the highest branching ratios have been achieved for dibenzoterrylene, where record values of up to 55% are reported for dibenzoterrylene in *p*-terphenyl nanocrystals.[21] The cases of anomalously high branching ratios for terrylene were only detected on annealed hBN. In fact, in our experiments not a single molecule with a 0-0 ZPL beyond 600 nm was detected without prior annealing of the hBN flakes. Annealing, at the temperatures we applied (500 ˚C up to 900 ˚C) is expected to remove most organic contamination[46] and to at most redistribute defects such as vacancies,[47] as the removal of structural defects would require much higher temperatures, up to 1700 ˚C.[48]

Remarkably, we also find considerably fewer molecules on the annealed samples, although we kept the sublimation rate of terrylene fixed or even slightly increased it. This is for example visible in the fluorescence image of an annealed flake in Figure 5.12. Compared to Figure 5.7a, there are significantly less emitters present on the flake. Moreover, the emitters that are there are mostly concentrated in the regions where the AFM scan shows an increased surface roughness. We propose as a possible explanation that terrylene anchors to (organic) contamination at the hBN surface. As annealing dramatically reduces the concentration of those anchors, terrylene molecules will either leave the flake area or may aggregate to the few nucleation sites and stop fluorescing because of self-quenching. Another possibility is that the annealing process creates dangling bonds at defect sites, which may react with terrylene upon sublimation and bleach them as a result. Interestingly, we find that the number of terrylene molecules on the flake increases again if prior to molecule sublimation, the annealed samples are intentionally contaminated by the spin-coating of n-hexadecane, which is known to form monolayers on top of hBN.[49] On the one hand, contamination could help terrylene to find more anchors and favor immobilization. On the other hand, contamination present before annealing could prevent terrylene from finding a site where it can interact strongly with the hBN, for example with some defect in the top hBN layer. We speculate that these hBN defects might be responsible for the red-shifted molecules. They would be accessible only after annealing of the hBN, right before the terrylene molecules are sublimated. However, binding to specific defects cannot explain the large inhomogeneous broadening on its own. In section 5.6, we propose that (local) strain, which could also affect atomic distances for defects, could be a possible explanation for the large inhomogeneous broadening when the molecule conforms to the strained hBN. This could point to a strong interaction with hBN, possibly in the form of chemisorption. For further studies, the need for special anchoring points could possibly be avoided by in-situ evaporation of terrylene on cold hBN surfaces, preferably performed in high vacuum and in-situ annealing of the surface. However, none of these steps are possible

in our setup. The nature of the defects that provide anchoring for terrylene could be also studied by intentionally creating defects in the lattice to see whether the concentration of the red-shifted molecules increases. However, the available methods to create defects also tend to create a lot of active emitters, and not only in the upper layer, such as observed with ion beams,[50] oxygen plasma[51] or with electron beams.[31]

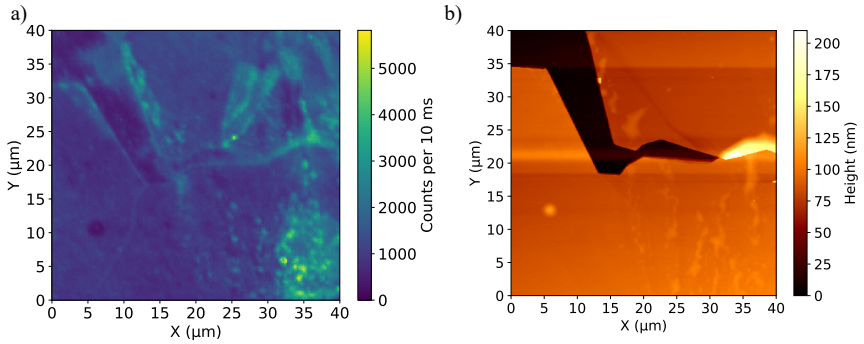

Figure 5.12.: (a) Fluorescence image and (b) AFM image corresponding to same area of a hBN flake that was annealed at 500 ˚C for 12 hours. The region in (a) for 25 < X < 30 µm and 23 < Y < 35 µm appears to have changed with respect to the same region in b), perhaps due to a folding of a part of the flake by the AFM tip.

5.3.4. SPECTRAL DIFFUSION

Apart from changes in the inhomogeneous distribution, we also find that annealing of the hBN flakes, prior to deposition of molecules, improves the spectral stability of the single emitters, reducing the number of (tunneling) two-level systems (TLSs). This observation is consistent with our hypothesis that these TLSs may have been located in the organic contaminants. The improvement of the spectral stability is most clear when we used an annealing temperature of 500 ˚C up to 750 ˚C, but much less clear for higher temperatures of up to 900 ˚C. An evident case of coupling of a molecule to a single TLS is shown in Figure 5.13a, which traces the 0-0 ZPL position over time at gradually-increased excitation intensities. In Figure 5.13b, the number of spectral jumps observed in a time window of 200 s is related to the power density of the laser spot at the position of the molecule and follows the same relation as the fluorescence intensity of the 0-0 ZPL. Therefore, these spectral jumps are laser-induced in one-photon processes. Later, we will show that the spectral jumps are also observed by resonant excitation, which requires power densities of at least two orders of magnitude weaker, due to the narrow width of the 0-0 ZPL with respect to the width of a vibronic transition.

In some experiments, we noticed that the spectral diffusion also depends on the location of the molecule. Figure 5.14 shows an example of the observed spectral diffusion of 0-0 ZPLs of single molecules with corresponding locations on the hBN

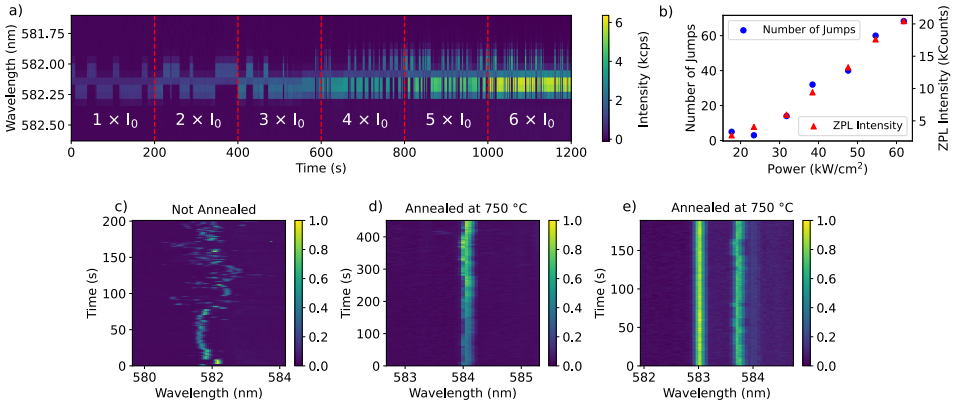

Figure 5.13.: A 0-0 zero-phonon line (ZPL) of a terrylene molecule in the main site followed for 20 minutes on an hBN flake that was annealed at 750 ˚C for 12 hours, excited by a vibronic transition with 532 nm light. The excitation intensity is raised after each frame of 200 s. The associated power densities, relative to the initial intensity I_0, are shown in (b), together with the number of spectral jumps that are observed in the 200 s time window and the integrated intensity of the 0-0 ZPL for a period of 1 s. Without annealing, the spectral time trace typically exhibits complex spectral diffusion as shown for example in (c). In this case, the molecule initially wanders around a relatively narrow spectral region, but extends over a much wider region from about 70 s. After annealing, the amplitude of spectral diffusion is typically strongly reduced, as in (d), even though the laser power is doubled at each 100 s interval. Some molecules do not show any spectral diffusion on the scale resolved by the spectrometer, as is the case for the leftmost molecule in (e). The spectra in (c) are measured on a different sample than the spectra in (d) and (e).

flake, depicted in the middle. The two left series of spectra were recorded around an outer edge and inner edge, possibly a step edge, and show apart from a higher concentration of emitters, an increased rate of spectral diffusion with a higher number of spectral positions. The stabler emitters were, however, found in the central regions of the flake, where the surface is generally flat, as shown before with AFM in Figure 5.5. Interestingly, a similar effect was observed by Noé *et al.*[52] for luminescent carbon nanotubes (CNT) that were grown onto an hBN substrate, and located either close to the edge or in the center regions. The stability of the emitter in the CNT was found to be much better in the center of the flake than close to the edge.[52] As a possible reason for this observation, Noé *et al.* pointed to a higher concentration of dangling bonds around the edges and possible accumulation of catalyst particles originating from the chemical vapor deposition of CNTs to contribute to fluctuations in charge. Unfortunately, in our case, the spatial resolution is limited by our confocal microscope, while Noé *et al.* could

observe the distance of their CNT from the edge by AFM imaging.

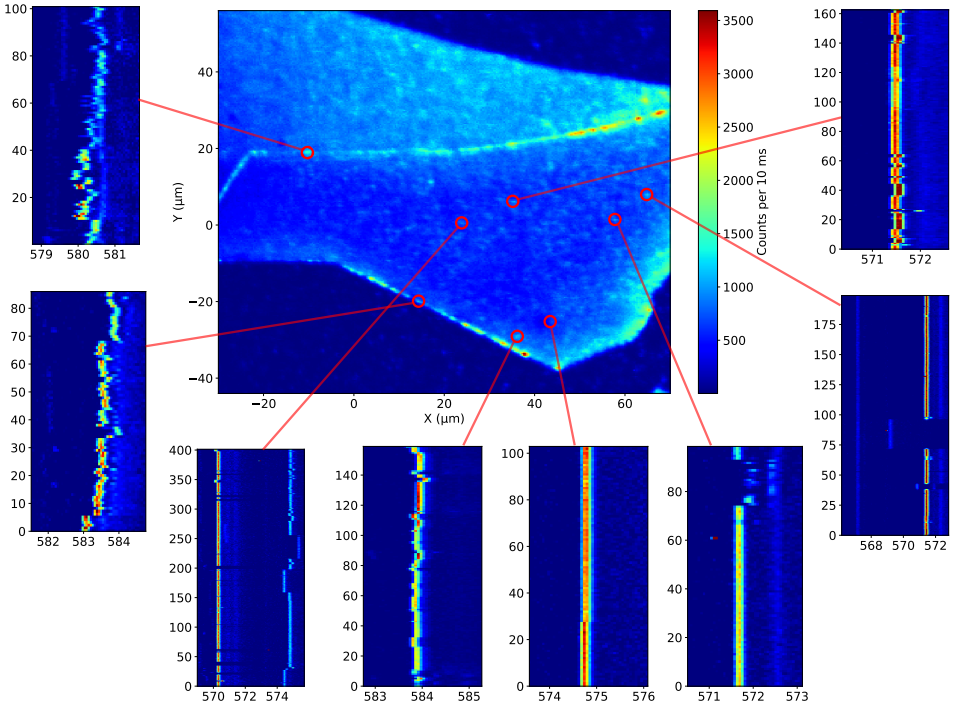

Figure 5.14.: Shown in the middle is a fluorescence image of an annealed (750 ˚C for 12 hours) hBN flake (NIMS, Japan). The red circles with connected lines correspond to the molecule(s) in the plotted series of spectra, with focus on the 0-0 ZPL. The two spectra on the left correspond to molecules located close to an edge, while the remaining spectra are recorded on extended terraces. The horizontal axes of the spectra correspond to the wavelength and the vertical axes correspond to the spectrum number, where each spectrum was integrated for 1 s with a 1200 lines/mm grating at a 96 µm slit size.

Whether the spectral diffusion that we observe is merely a charge-induced phenomenon, as explained by Noé *et al.*, seems unlikely, based on our previous observations, such as an increased spectral diffusion upon a re-contamination of the surface with *n*-hexadecane and the effect of thermal annealing. Other sources, beyond remote TLSs, were considered as well, such as a slow spatial diffusion of the molecule itself, over the surface. As an initial test, we monitored the polarization of the molecule's fluorescence with a polarizing beam splitter, to observe both the horizontal and vertical component. The relative intensities of these two components showed that there was no

change in the angle of terrylene's long axis (Figure 5.15a and 5.15c). However, without rotation, translational motion is still a possibility. To consider translational motion, we recorded confocal images of two molecules over the course of 90 minutes and fitted their point-spread functions (PSF) to obtain a measurement of distance between the two molecules over time. The position of both molecules was deconvoluted by fitting the PSF to a 2D Gaussian of the form:

$$G(x, y) = B + A \exp\left(-((x - x_0)^2 + (y - y_0)^2)/\Sigma\right). \tag{5.2}$$

The term B resembles the background counts, A the amplitude of the PSF, x_0 and y_0 the position of the molecule and Σ the spread of the PSF. The results of the distance between the two molecules, as obtained from the PSF fits, is shown in Figure 5.15g and shows that there is no clear departure from the mean, as expected from random walk behaviour. Hence, if there is any spectral diffusion at all, it is likely very limited. Another source that we checked is the substrate. For defects in hBN, it was shown that coating the silica substrate with a thin layer of alumina would substantially reduce the spectral diffusion,[12] through surface passivation. However, their hBN was only 13 nm thick and thus the emitters, not necessarily present in the top layer, would be much closer to the substrate. Still, we tested whether a sapphire substrate would result in stabler emission, but this is not the case. Finally, we could rule out influences of the substrate on the spectral diffusion when we found an hBN flake that did not completely attach to the substrate. The molecules located on the free-standing part of the flake were still equally unstable as the molecules that were located on the attached part.

Thermal annealing, before deposition of molecules, is the only method that consistently improved the spectral stability of the molecules. In general, we observe a decrease in the number of spectral positions, while also the amplitude of spectral diffusion decreases (Figure 5.13a, 5.13d and 5.13e). Without annealing, the spectral jumping is in general much more complex, consisting of many, possibly coupled, levels, whose population rates could change over time (Figure 5.13c). The scale of the spectral jumps, extending up to a few THz in some cases, and the lack of correlation between spectral diffusion of emitters in the same focal area, points to events in the close vicinity of the molecule. As discussed before, the molecule is likely anchored to (aggregates of) contaminants on the surface or possibly to a defect itself. This (nonfluorescent) contamination itself can be responsible for the spectral jumps, i.e. by a group of atoms tunnelling between two spatial positions, perturbing the optical transition of the terrylene molecule by the electrostatic or elastic dipole-dipole interaction. The contamination likely nucleates around an hBN defect and could explain why we observe more spectral diffusion, as well as more terrylene molecules that anchor to the surface, in the more defect-rich edges of the hBN, as in Figure 5.14. However, the exact nature of these TLSs remains unknown due to the random environment around the molecule.

5.3.5. RESONANT EXCITATION OF THE 0-0 ZPL

The work that I presented so far only shows molecules that were excited by a vibronic transition and not resonantly through the narrow 0-0 ZPL. Moreover, the 0-0 ZPL linewidth resolved in the emission spectrum is limited by the spectrometer resolution

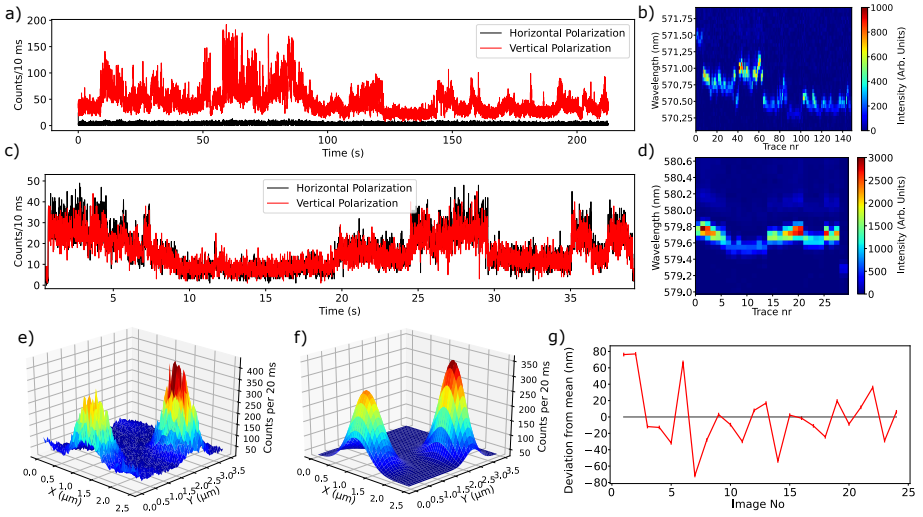

Figure 5.15.: a,b) Fluorescence time trace and spectra of a molecule whose fluorescence is nearly perfectly oriented with the vertical polarization component. Spectral jumps during the time trace have no influence on the horizontal polarization component. c,d) Shows the time trace and spectra of another molecule with comparable intensities in both polarization channels. Also here the spectral jumps have no influence on the ratio of the two polarization components. Around 28 s, the molecule jumps to a spectral position where the excitation was much less efficient, the signal dropped considerably, and therefore the data was cut here. The spectra in b) and d) were recorded with a 1 s integration time. The time scales of the fluorescence time trace and of the spectra are different, due to some delay between the recorded spectra. Panel (e) and (f) show respectively the experimental and fitted point-spread functions of two molecules that are approximately 2 µm apart from each other and do not (or barely do) overlap with the PSFs from other molecules. A single scan consisted of 100x100 pixels over a range of 5x5 μm^2 and took about 200 s to acquire with the scanning mirror. In total, 24 of these images were acquired over the course of 90 minutes with short pauses in between. Panel (g) shows the distance between the two molecules extracted from 24 consecutive confocal images, as in panel (e). The average error of the fit is just a few nm, but the measurements likely have a larger error due to spectral jumps occurring while recording the PSF. For all fitted data, the distance appears to revert around a mean value of 2.18 µm, and shows no clear trend. Hence, if there is any spatial diffusion, its extent is very limited.

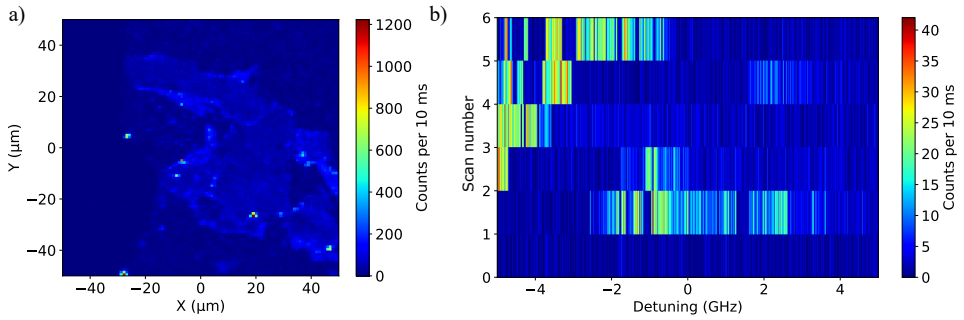

Figure 5.16.: a) Confocal fluorescence map of a collection of hBN flakes, taken at an excitation wavelength of 582.38 nm at a relatively high laser intensity of 350 W/cm^2. The brightest spot, around (X = 20, Y = -25) corresponds to the emission of the molecule in Figure 5.18. b) Common behavior of a molecule shown in a series of excitation spectra. The series of spectra were taken with the procedure mentioned in the text. In the second line of the scan, the laser was pointed to the position of the molecule. The strong spectral diffusion and blinking makes it difficult to extract a linewidth from this measurement.

(51 ± 3 GHz per pixel), while the linewidth of terrylene is expected to be up to three orders of magnitude narrower, around 45 ± 3 MHz, if it is limited by the measured fluorescence lifetime of 3.6 ± 0.2 ns. With a tunable dye laser (linewidth of a few MHz) we excited terrylene molecules resonantly. In many cases, the molecule jumped out of resonance with the excitation laser, already in the first scan or the molecule showed such strong spectral diffusion that the molecule appeared intermittently over the full scanning range (Figure 5.16b). With lower excitation intensities of a few W/cm^2, we could follow the molecules longer. A procedure that worked well consisted of tuning the laser to some wavelength around the peak of the inhomogeneous broadening (Figure 5.10a and 5.10c) and record a fluorescence map of the flake, covered with a high concentration of terrylene. The molecules that are in resonance with the excitation laser will appear as bright spots on the flake region, as shown in Figure 5.16a. Then we start a scan of the laser and while it is running we move the laser to the position of the molecule.

For the remainder of the molecules, not showing behavior as in Figure 5.16b, it was possible to extract a linewidth of the 0-0 ZPL. In general, a Lorentzian distribution fits best to the excitation spectrum's profile (Figure 5.17d). However, in some exceptions, possibly due to fast spectral diffusion, a Gaussian distribution provided a better fit, such as in Figure 5.17b. One of the narrowest linewidths that we could find is shown in Figure 5.17d. In this figure, the Lorentzian fit extracts a linewidth of 390 ± 10 MHz, which is less than a factor 10 away from the lifetime-limited linewidth of 45 ± 3 MHz. Furthermore, the molecule has a resonance split into two Lorentzian distributions that are separated by 1.1 GHz. This could be the result of a fast-switching two-level system.

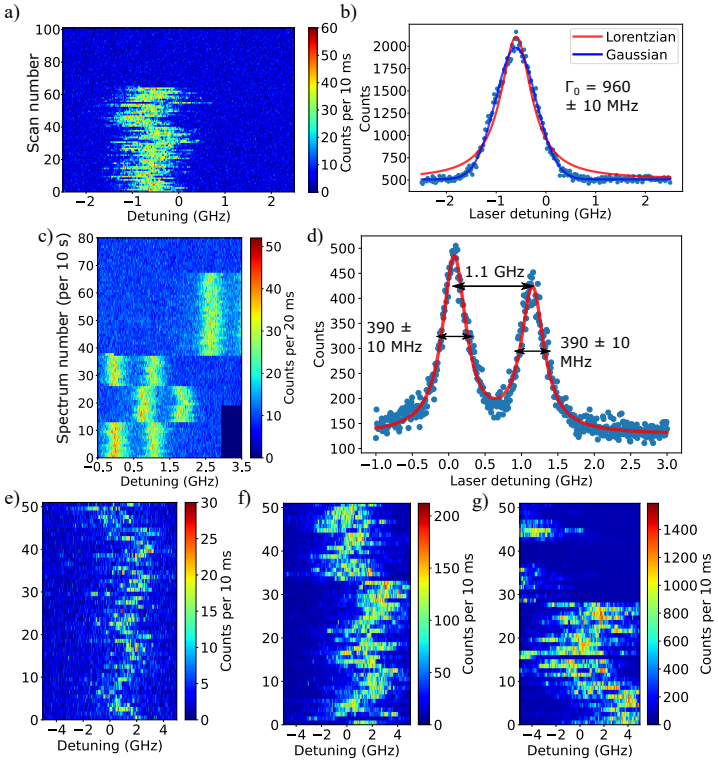

Figure 5.17.: (a) Series of excitation spectra of a molecule at 581.96 nm, taken with 11 W/cm^2 laser intensity. (b) The summed intensity of all the spectra in (a) builds up the figure. The excitation spectrum is fitted with both a Lorentzian and Gaussian distribution. The Gaussian distribution fits best and yields the indicated linewidth. (c) One of the narrowest resonances that are found on hBN is shown in this series of excitation spectra. (d) A fit of two Lorentzian distributions for the two resonance lines present in (c). (e), (f), (g) Spectral diffusion of a molecule recorded at increasing excitation intensities of 1 W/cm^2 in (e), 14 W/cm^2 in (f) and 250 W/cm^2 in (g).

At longer timescales, the molecule also jumps to different spectral positions and jumps out of the scan range after about 10 minutes. This behavior is very common and happens for instance also for the molecule in Figure 5.17c. In rare cases, the molecule stays within the scan region or can be recovered by slightly adjusting the center of the scan. The molecule in Figure 5.17e, 5.17f and 5.17g remains within the scan region, but shows an increasing spectral wandering upon an increase of the excitation laser intensity. A broadening of the linewidth is expected with a higher laser intensity, but the extent of broadening is further increased by a photo-induced spectral diffusion.

The most stable molecule that we found is shown in Figure 5.18a. This molecule

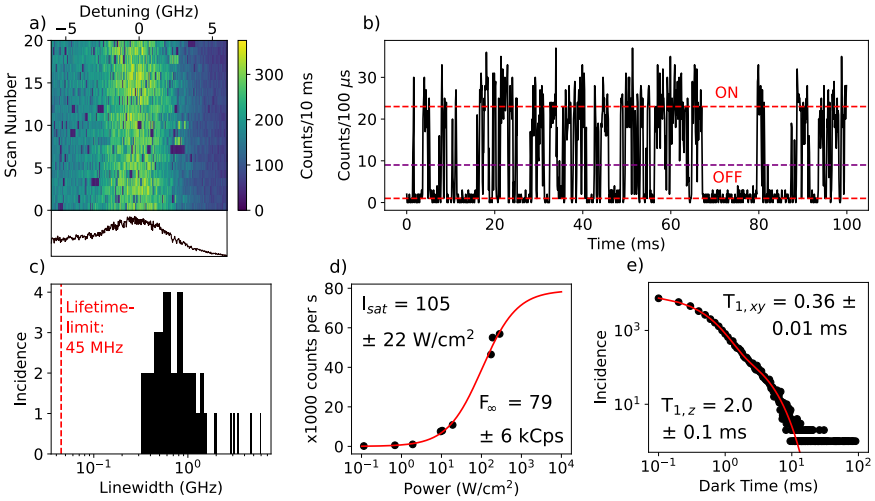

Figure 5.18.: a) Excitation spectrum of the 0-0 ZPL of a single molecule that did not jump out of resonance with the laser, even at higher excitation intensities. The homogeneous linewidth is about 4.7 ± 0.3 GHz and is measured with a scan rate of 5 seconds per row. The line plot underneath the figure shows the asymmetric profile of the 0-0 ZPL. A time trace of the fluorescence signal of this molecule in (b) shows characteristic quantum jumps due to intersystem crossing to the triplet state. However, in some cases the molecule remained dark for much longer times than the triplet lifetime, as is also visible in (a). These long dark times may be attributed to a relatively short spectral jump back and forth between another (out-of-range) spectral position. The purple line represents the threshold set between the ON and OFF state of the fluorescence. c) Distribution of 0-0 ZPLs linewidths found for molecules on different flakes. The red dashed vertical line represents the lower limit set by the fluorescence lifetime. Due to the large distribution of linewidths, the horizontal axis has been set to a logarithmic scale. d) Saturation curve of the fluorescence of the molecule in (a), fitted with $F(I) = F_\infty(I/I_s)/(1 + I/I_s)$, where I_s is the saturation intensity of the laser and F_∞ is the maximum fluorescence rate. The saturation intensity is 105 ± 22 W/cm^2, 2 orders of magnitude larger than typically obtained with our setup for near-lifetime-limited emitters. This is explained by the 2 orders of magnitude broader linewidth, as the saturation intensity scales linearly with the linewidth of the transition. e) Distribution of dark periods in the resonance fluorescence signal, recorded over 60 s with 100 µs time bins (as in (b)). The characteristic timescales of the fit (red curve) are shown on the top right and bottom left.

remained at the same resonance frequency, regardless of the excitation intensity. The molecule has a relatively broad linewidth of 4.7 ± 0.3 GHz and an asymmetric profile of the 0-0 ZPL, as shown in the bottom plot of Figure 5.18a. The asymmetric profile might be the result of spectral diffusion to one side. As the molecule remained in resonance, we could record a fluorescence time trace at resonance with the 0-0 ZPL, as shown in Figure 5.18b. The time trace shows quantum jumps that can be assigned to intersystem crossing. The blinking events of longer duration, extending up to tens of ms, are likely from another source, such as jumps back to and from another out-of-range spectral position. To analyze the characteristic time scales of these quantum jumps, we determined a threshold between the ON and OFF state, where a crossing of this threshold would indicate a change from ON to OFF or vice versa. For a time trace of 60 s, the lengths of the period where the molecule was OFF are plotted into a histogram, shown in Figure 5.18e. The histogram is best fitted by a bi-exponential decay, with characteristic triplet lifetimes of 360 ± 10 µs and 2.0 ± 0.1 ms. We attribute the short decay time to the indistinguishable decays of the in-plane triplet states T_{xy}, while the remaining long decay corresponds to the out-of-plane state T_z.[53] The triplet lifetimes agree well with terrylene in the extensively studied hosts *p*-terphenyl[54–56] and anthracene.[57]

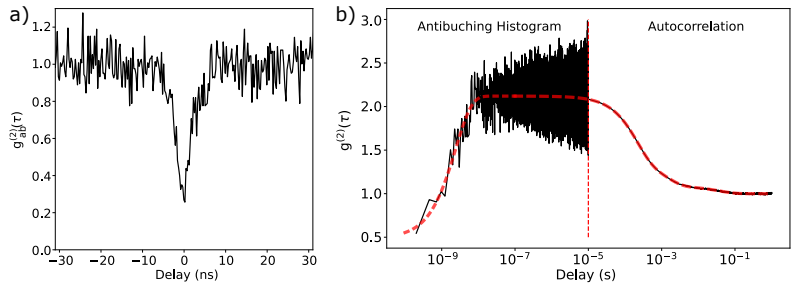

Figure 5.19.: Normalized antibunching histogram of the molecule in Figure 5.18a, measured at resonance with the 0-0 ZPL. No Rabi oscillations are present, but the characteristic time of the exponential increase to unity is shorter than for the off-resonant excitation, indicating that stimulated emission reduces the antibunching time scale. b) The full extent of the correlation function is composed for the left side by a renormalized antibunching histogram and for the right side by the calculated autocorrelation of the fluorescence signal, both recorded with an excitation intensity of around 100 W/cm^2 (see Figure 5.18d for reference).

We continued by recording an antibunching histogram of the resonance fluorescence (Figure 5.19a). No Rabi oscillations are observed in the histogram, which is expected when the linewidth is significantly broadened by dephasing. The measured linewidth of 4.7 ± 0.3 GHz would correspond to a lower bound of the decoherence time T_2 of about 68 ± 4 ps. Combined with the autocorrelation of fluorescence, recorded with 10 µs time bins, we could renormalize the antibunching histogram and extend the full autocorrelation to over 9 orders of magnitude in time (Figure 5.19b).

Although we extensively studied terrylene as a model molecule for characterizing hBN as a potential host, we have tried to measure several other molecules on hBN. The convenience of terrylene emerged particularly due to its broadband absorption at the fixed 532 nm wavelength of the excitation laser, while this was not the case for many other molecules. In this part of the chapter, I will show results of the other molecules that we measured and were either intentionally or unintentionally placed on hBN.

5.4. BEYOND TERRYLENE: OTHER MOLECULES ON HBN

5.4.1. MOLECULE X

On the samples that were prepared by spin coating fluorescent molecules on the hBN flakes, there was regular contamination with fluorescent impurities. One of these impurities, sometimes denoted as molecule X, is particularly present in polymers[58] and solvents,[59] such as toluene.[60] The latter is the solvent that we use in our spin-coating procedure as a transfer solvent for other fluorescent molecules. A spectrum of molecule X on hBN is shown in Figure 5.20 and has the same vibrational fingerprint as found in the literature. Similar to terrylene, the 0-0 ZPLs of these impurity molecules were found over a broad range of wavelengths, extending from 618 nm up to 640 nm, for the 24 molecules that we measured. Similar to terrylene, this wide range of wavelengths for the 0-0 ZPLs of molecule X designates a large inhomogeneous broadening.

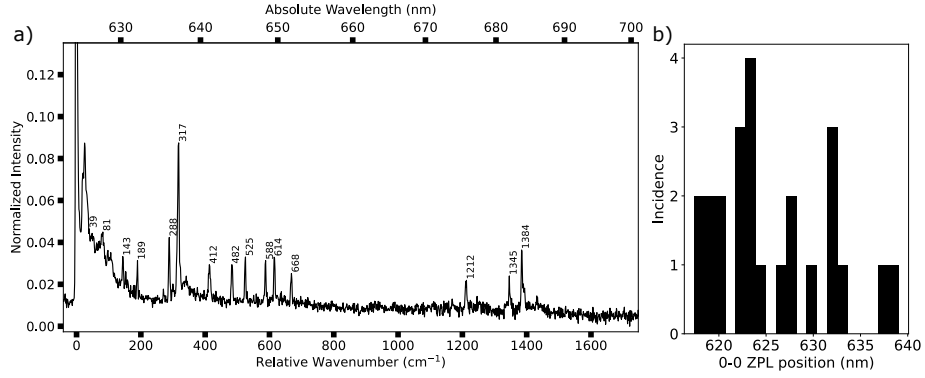

Figure 5.20.: (a) Fluorescence emission spectrum of molecule X with annotated vibrational peaks, normalized to the intensity of the 0-0 ZPL. The excitation frequency was 532 nm. (b) Histogram of the location of the 0-0 ZPL of 24 molecules that shared the vibrational fingerprint as in (a).

As this molecule arises from contact with organic solvents, it can easily end up on the hBN upon "cleaning" it with solvents. There are several reports of emission from hBN, attributed in the papers to defects, that have a similar emission peak.[8,61] The paper by Ronceray *et al.* treats the activation of emission from hBN by solvent molecules that are possibly binding to hBN surface defects, as the measurements takes place with

hBN submerged in organic solvents. Interestingly, the observed peak of the emission spectrum is in the same region as molecule X. The paper also describes that this effect is observed in many other organic solvents. The fluorescent impurity molecules in those solvents may bind to the hBN, giving off clear point-like emission in wide-field images as they stay longer in one place. Ronceray's reported mechanism of emission, if truly from fluorescent organic impurities in solvents, is interesting. It shows that molecules may possibly prefer to bind to surface defects than on pristine hBN. Therefore, it would be interesting to repeat their experiment with a known dye dissolved in the organic solvent, such as terrylene.

5.4.2. GRAPHENE QUANTUM DOTS

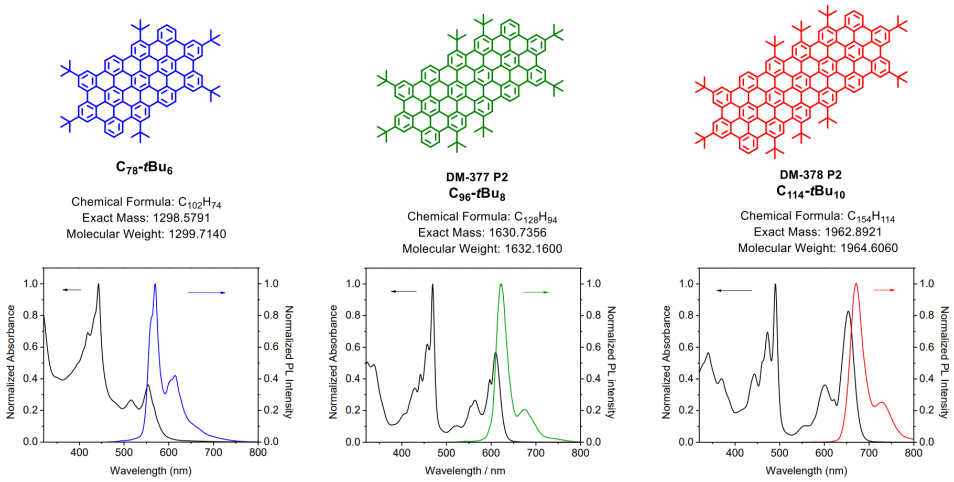

Figure 5.21.: Shown on the top are the chemical structures of the three graphene quantum dots with below their corresponding absorption (black) and fluorescence emission spectra (in color). The image was provided to us by the group of prof. J.S. Lauret from Paris Saclay university. The spectra were measured with 1,2,4-trichlorobenzene as the solvent.

Apart from unintentionally placed molecules, such as molecule X, we also performed experiments on a novel family of fluorescent molecules, namely graphene quantum dots (GQDs), in the shape of ribbons (see structures of the three types in Figure 5.21). These molecules were synthesized at Paris Saclay university[62] and studied by the research group of prof. J.S. Lauret for their strongly fluorescent properties.[63,64] So far, observing narrow spectra of the GQDs at low temperature is a challenge. A measurement of triangular GQDs in a polystyrene matrix showed broad emission lines that did not reveal the fine structure of the emission spectrum.[65] The GQD molecules are much bigger than the typical aromatic fluorescent molecules used in single-molecule spectroscopy, and thus finding a suitable host for them to obtain significant line-narrowing of the emission

spectra is a challenge. Apart from the flat ribbon structure there are tert-butyl chains that prevent the molecules from aggregation and thus promote solubility. As such, the molecules could be easily dissolved in toluene. Subsequently, with the GQDs diluted to sub-nM concentrations, we could spin coat them onto annealed hBN flakes. At room temperature, the molecules are easily found using an excitation wavelength of 532 nm. In particular, we focused on the C78 and C96 GQD, where the number represents the amount of carbon atoms present in the aromatic part of the molecule, thus excluding the chains. The room-temperature emission spectra of these two types of GQDs, in ensembles, are shown in Figure 5.22 and reveal that the emission peaks and structure of the spectra are similar to those observed in a 1,2,4-trichlorobenzene solution.

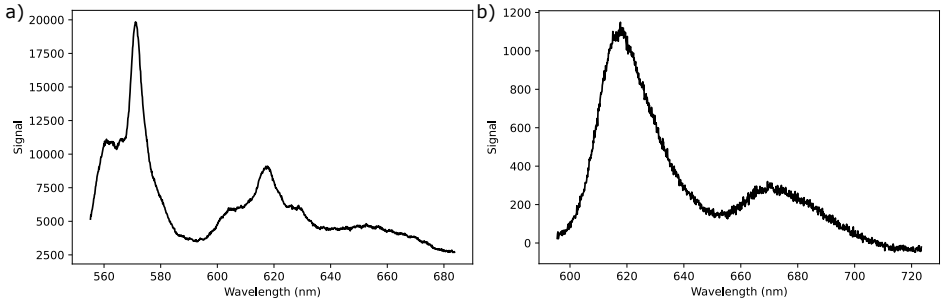

Figure 5.22.: Fluorescence emission spectra of ensembles of respectively the C78 GQD in panel (a) and the C96 GQD in panel (b). Both spectra were taken at room temperature with a 532 nm excitation laser. The spectrum in (a) peaks around 571 nm and the spectrum in (b) has a peak around 618 nm.

Upon cooldown and subsequent line narrowing, the signal from the GQDs was diminishing, probably due to weak or no absorption at all around 532 nm. To improve the signal we required the dye laser for excitation. The dye laser is best optimized for use with the C96 GQD, where a good absorption was measured for some molecules around 570 nm. In the case of Figure 5.23a, the 0-0 ZPL of the C96 QGD is around 615.8 nm, excited with 570.54 nm. The difference of 1288 cm^{-1} is close to the series of vibrational lines around 1300 cm^{-1} in the emission spectrum. The spectrum in Figure 5.23a and 5.23b is likely from a single molecule, as at some point the molecule jumped out of resonance and the signal was lost. The spectra are characterized a large number of vibrational modes, with most of them at low frequency. In part, this could be due to the large size of the molecule, as the number of vibrational modes scales with the number of atoms, while the large size of the molecule can also decrease the energy of some modes. The strongest mode around 128 cm^{-1} in Figure 5.23b is, analogous to the extension mode in other aromatics, where the molecule's length oscillates around equilibrium. For the C78 GQD we were only able to detect a signal at elevated temperatures of around 80 K. Due to the broadened spectrum it is difficult to resolve the vibrational spectrum of this molecule, as shown in Figure 5.23c.

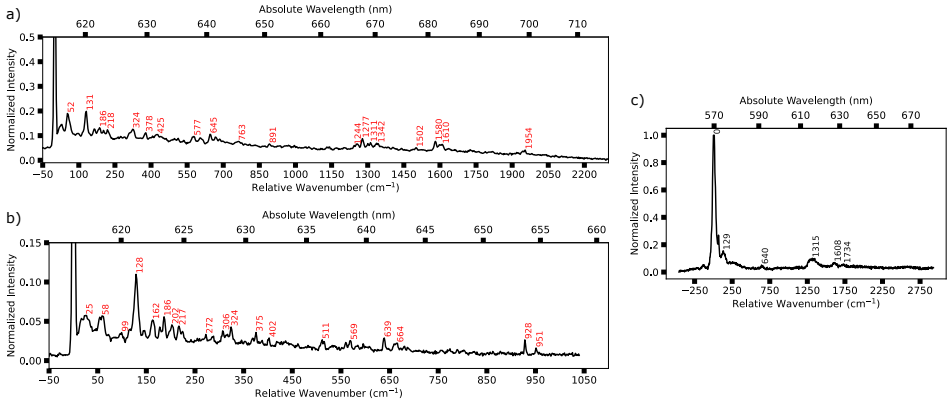

Figure 5.23.: Panel (a) shows the full emission spectrum of the C96 GQD at 2 K, excited at 570.74 nm and taken with a 600 lines/mm grating at a 0.1 mm slit size. The higher resolution spectrum, taken with a 1200 lines/mm grating and a 0.1 mm slit size, is shown in panel (b). In panel (c) an emission spectrum of the C78 GQD is shown, which was only observed at elevated temperatures. In this case the temperature is around 80 K and is responsible for the broadened linewidth. The C96 GQD molecule in (a) and (b) has a 0-0 ZPL around 615.8 nm and the C78 GQD molecule in (c) has a 0-0 ZPL around 569.7 nm.

The spectra of GQDs on hBN show that hBN is a promising host for other molecules than only terrylene. In particular, the notion that hBN can be applied for rather bulky molecules such as GQDs may underpin the universality of hBN as a host matrix for fluorescent molecules. Moreover, many properties of these GQDs are still unknown, such as their photophysical parameters (triplet blinking) and could in best case, such as for terrylene in Figure 5.18, be studied at the single-molecule level. However, it is very important to consider what excitation wavelength is optimal for each type of molecule. In addition, GQDs (and molecule X) are showing the same type of spectral diffusion as observed for terrylene, which can quickly move the molecules out of resonance with the laser. Terrylene, on the other hand, stayed most of the times in resonance with the 532 nm laser. As a possible solution for the elimination of spectral diffusion we considered adding another layer on top of the hBN, thus encapsulating the molecules.

5.5. ENCAPSULATION OF TERRYLENE

5.5.1. TRANSFER OF LARGE AREA HBN

In case the spectral diffusion is primarily caused by degrees of freedom for the organic contamination present on the surface, then perhaps this spectral diffusion could be suppressed by passivating the environment through encapsulation by another hBN layer. In fact, encapsulation by hBN is already a common procedure to for example improve

the linewidth of emission from excitons in transition metal dichalcogenides (TMDs).[66,67] The encapsulation of large structures such as TMDs is not difficult, but for small-sized molecules, such as terrylene, the encapsulation could push away the molecules. This self-cleaning method is in most cases desired for having a clean interface in stacked structures. As mentioned in section 5.3.1., the encapsulation may also cause pile-up of residues and our fluorescent molecules into air pockets/bubbles.[28] Intuitively, the encapsulation could be best performed with a thin layer or monolayer of hBN, to have easier adaption of the top layer to the part to encapsulate, without exerting much pressure on the bottom hBN. To this end, we used 13 nm hBN grown by chemical-vapor deposition onto a copper foil (obtained from the company Graphene Supermarket). The copper foil can be slowly (typically less than an hour) dissolved in an etchant solution (10% ammonium persulfate in water). As the copper is dissolved, a slide of teflon with a hole in the middle floats in the water and creates surface tension (Figure 5.24a), which will keep the hBN floating on the water surface after the copper is completely dissolved. Then the sample is slowly pushed towards the water and the whole layer attaches to the substrate as it gets into contact. The procedure for hBN transfer from copper foil is based on this work.[68] Although the transfer was successful and allowed the encapsulation of many flakes at once (the monolayer can be millimeters large, see Figure 5.24b), this rather "dirty" method left behind a lot of emission on our samples, which made it difficult to distinguish emission from terrylene.

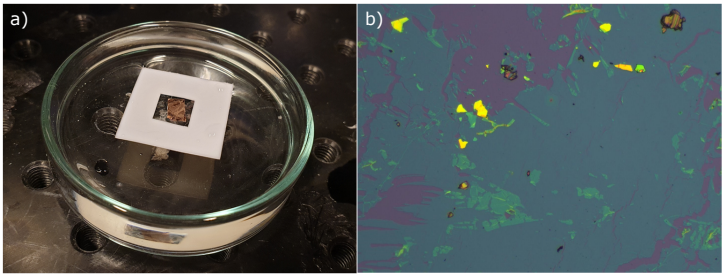

Figure 5.24.: Panel (a) shows a piece of copper foil, coated with a 13 nm thick hBN layer, floating in the middle of a hole in a Teflon slide that also floats on an etchant solution of 10% ammonium persulfate in water. Panel (b) shows hBN flakes on a substrate (most of them in yellow or green color), with areas that are encapsulated covered by a bluish film. Note that upon transfer the sheet tears and does not cover all parts of the substrate.

5.5.2. FLAKE-ON-FLAKE ENCAPSULATION

Another method for encapsulation is the use of the stamping technique. This method is very similar to exfoliation in the sense that a polymer layer (polycarbonate (PC) or PDMS) is used to pick up a flake (for example from a substrate or exfoliated on tape) and positioned above (using a microscope that has two independent micromanipulators) and pushed towards another flake that is already on a substrate.

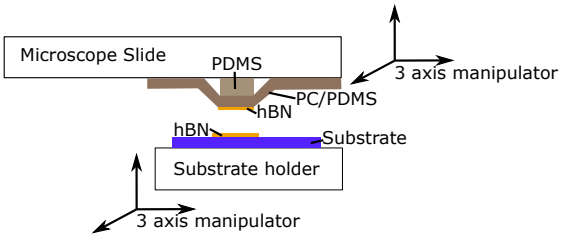

Figure 5.25.: Schematic of the stamping procedure with two microscope slides connected to individual micromanipulators. The substrate with the exfoliated hBN is attached to a substrate holder by vacuum. A microscope slide is prepared with a small piece of PDMS gel (from Gel-Pak) to support a layer of polycarbonate (PC) or PDMS tape (from Gel-Pak as well), with exfoliated hBN attached to it. The manipulators can be used to position the two flakes on top of each other and to approach.

The procedure for stamping of hBN flakes, and many other 2D materials, is schematically shown in Figure 5.25. The hBN for transfer is prepared by the scotch-tape method, as described before. A piece of PC or PDMS tape is then pressed on the scotch tape, such that some hBN flakes attach to it. Subsequently, the PDMS tape is fixed to the microscope slide, where the PDMS gel makes sure a part of it is suspended. This needs to be the region with the flakes of interest present. The flake to transfer is then positioned on top of the flake that needs to be covered and the two flakes are moved towards each other until there is slight contact of the film with the substrate. Subsequently, the sample is heated till 60-90 ˚C, such that thermal expansion creates full contact between the PDMS or PC film and the substrate. Then the sample is cooled back to room temperature, while the thermal contraction makes the film lose contact again with the substrate. When transfer of the flake was not successful the procedure was repeated with or without some minor changes in the parameters.

The result of the encapsulation using the stamping method is shown in Figure 5.26a and 5.26b. When the molecules are encapsulated, annealing was not performed anymore. However, we could anneal the bottom flake before deposition of molecules and encapsulation, as was done for the flake in Figure 5.26b. Interestingly, we found a large number of terrylene molecules on the non-annealed flake in the encapsulated part, but only one terrylene molecule was found on the encapsulated part of the annealed flake. Moreover, the background fluorescence was much higher for the case of the annealed bottom flake. This could be a result of the annealing, which may cause the formation of molecule emitters due to the presence of organic contamination between the interface of silica and hBN.[15] However, none of this emission was narrow at low temperature. The narrow emission that we could find was due to the presence of terrylene. However, the spectral diffusion is still a problem in the encapsulated areas of the hBN flake, as shown in Figure 5.27. The only molecule that we could find on the annealed flake, covered by a non-annealed flake, shows spectral diffusion (Figure 5.27a). Similarly, the

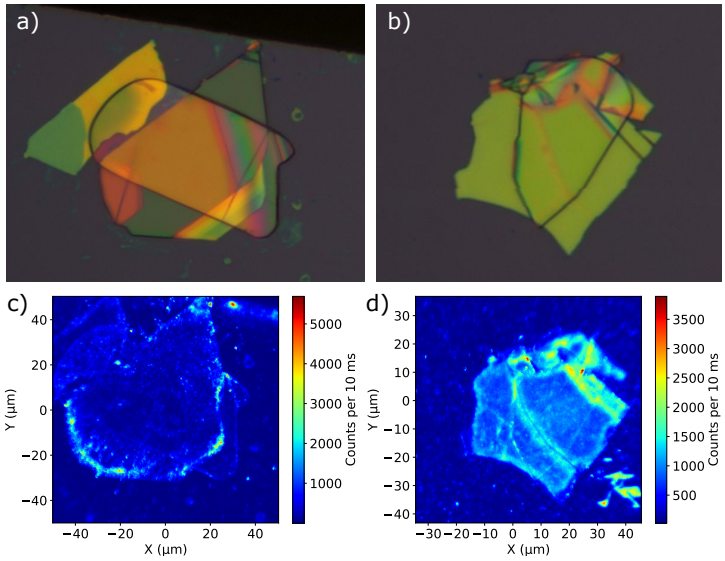

Figure 5.26.: Examples of encapsulation of an hBN flake by another flake of hBN, by the stamping method. In panel (a) the bottom hBN was not annealed and in panel (b) the bottom hBN was annealed. In both cases, molecules were deposited by sublimation before encapsulation (and annealing). The corresponding fluorescence maps of the flakes in (a) and (b) are respectively shown in panel (c) and (d). Note that the background is much higher for the annealed flake (d) compared to the non-annealed flake in (c). Hundreds of terrylene molecules were found on the non-annealed flake, while only a single terrylene molecule was found on the annealed flake.

molecules on the non-annealed flake show spectral diffusion as well (Figure 5.27b and 5.27c), on a scale that we regularly observe on non-encapsulated hBN flakes. Hence, the encapsulation of the molecules does not seem to improve the spectral stability, which might be due to the pile-up of contamination in areas where terrylene is also located. Of course, many parameters in the preparation of these encapsulated samples can be varied and may lead to different results. This can be for example the amount of force that we exert during stamping or the amount of heating we provide to make the top layer stick well.

There are possibly alternatives to the encapsulation methods that we used so far. This could be for instance exfoliation in a high vacuum environment, to keep all the layers in very clean condition. This could be combined with in-situ evaporation of the fluorescent molecules on a cold hBN surface. However, this would require sophisticated equipment. Another appealing alternative is the use of boron nitride nanotubes, which have proven to be able to encapsulate dye molecules and protect them from photodegradation at room temperature.[69]

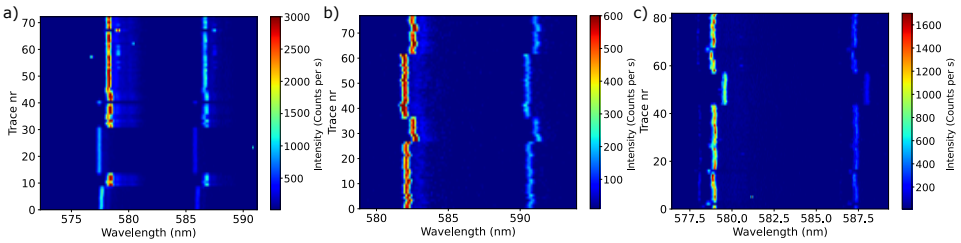

Figure 5.27.: Series of emission spectra of encapsulated molecules. The molecule in panel (a) was located in the encapsulated part of the annealed bottom flake. It was also the only molecule that we could find on this sample. Panel (b) and panel (c) show examples of spectral diffusion that we observed for molecules that were located on the non-annealed hBN flake, inside the encapsulated region.

5.6. WHAT CAN WE LEARN FROM THE LITERATURE ON HBN 'DEFECTS'?

Although the origin of emission of many emitters associated to hBN is unknown and some of them are disputed to originate from defects, but possibly organic molecules, we can still learn from the various experiments that have been undertaken to improve the emitter's quality and tuning of its properties. In particular, if the experiments are indeed performed unintentionally on molecule emitters, the experiments are very relevant.

Comparing the spectral properties of single terrylene molecules on hBN to the properties of hBN emitters, the similarities are striking. Homogeneous linewidths of about 1 GHz on average are also typical for other reported emitters associated to hBN.[38,39,70,71] Moreover, spectral diffusion, large enough to observe with a spectrometer, is also frequently reported for hBN emitters.[12,38,39,71–73] Methods of improvement for the quality of hBN emitters could therefore be possibly applied to our molecules as well. In the following part, I will show two experiments from the literature that are interesting candidates for follow-up experiments for terrylene on hBN, which we have tried to build up as well.

Interesting work by the group of Atwater[74] shows that high electric fields can improve the spectral properties of an hBN emitter, leading to almost lifetime-limited linewidths. This improvement was achieved by creating a heterostructure of graphene/hBN/hBN/graphene, where both graphene layers would act as independent electrodes, while the emitter was located in one of the hBN layers (or between). The explained mechanism of their work is that the very high electric field, in the order of 1-2 MV/cm, would deplete charge traps in the hBN, causing a strong reduction in charge noise, analogous to reports on the reduction of charge noise in semiconductor quantum dots using electric fields.[75] Even more surprising is the measured temperature dependence of the linewidth. The linewidth of the emitter is still below 1 GHz at a

temperature of 100 K, while the broadening is purely phonon-induced and lacks a linear component, i.e. a pure T^3-dependence. This could suggest that the electric field greatly suppresses the activity of two-level systems (TLSs) at higher temperatures as well, and cancels the linear broadening term that we also observe for our molecules. In section 5.5 we have shown that it is possible to encapsulate molecules between hBN. However, there is no definitive proof that the molecules are indeed in the encapsulated region. With a similar stack of hBN encapsulated molecules between graphene electrodes we could also prove that the molecules are really in-between the hBN flakes when their fluorescence is not quenched through contact with the graphene.

We also tried to make a similar heterostructure of hBN in between graphite (or multilayer graphene) electrodes (Figure 5.28a). In the first attempt we noticed that the thickness of the top graphite layer is very important for the measured fluorescence. If the layer is too thick, the fluorescence cannot penetrate the layer, as well as excitation light is only weakly transmitted (absorption is about 2.3% per layer in the visible). Consequently, the area where all layers overlap does not show any fluorescence (Figure 5.28b).

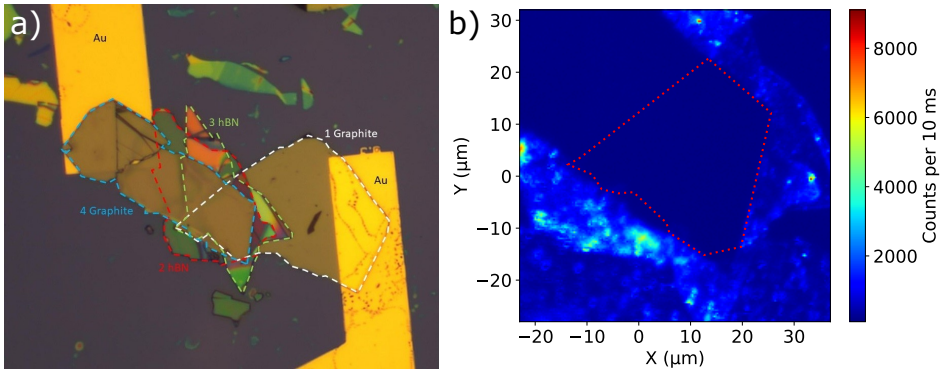

Figure 5.28.: a) Microscope image of the heterostructure with at the bottom a layer of graphite in contact with one of the gold electrodes. Followed by two hBN flakes on top of each other, with molecules deposited in between and a top graphite layer connected to the other electrode. Panel (b) shows the fluorescence image of the region where all layers overlap, bordered with a red dashed line. The fluorescence signal in this region is very weak, which is possibly due to the low transparency of the top graphene layer. See also the low contrast on the left electrode in (a), where the top graphene layer overlaps with the highly-reflecting gold.

With a thinner graphite layer, as shown in Figure 5.29, we were able to detect some fluorescence within the overlap region. However, the signal was relatively weak and recording a spectrum required an integration time of about 30 seconds at a high excitation intensity (> 100 kW/cm^2). Consequently, the spectrum of the terrylene molecules is less

well visible due to overlap with strong Raman signals from graphene. No spectral shift or stabilization of the fluorescence signal was observed on the spectrometer. This could be related to the intensity of the field, which depends on the voltages applied (10 V over the junction area) and the thicknesses of the hBN layers. However, the fact that we can detect fluorescence from single terrylene molecules indicates that the emitters are not quenched by the graphene and are likely located between the hBN layers. With better control over the thicknesses of the hBN layers and the top graphite layer the experiment can be improved, while spectral shifts are more easily visualized by resonant excitation of the 0-0 ZPLs.

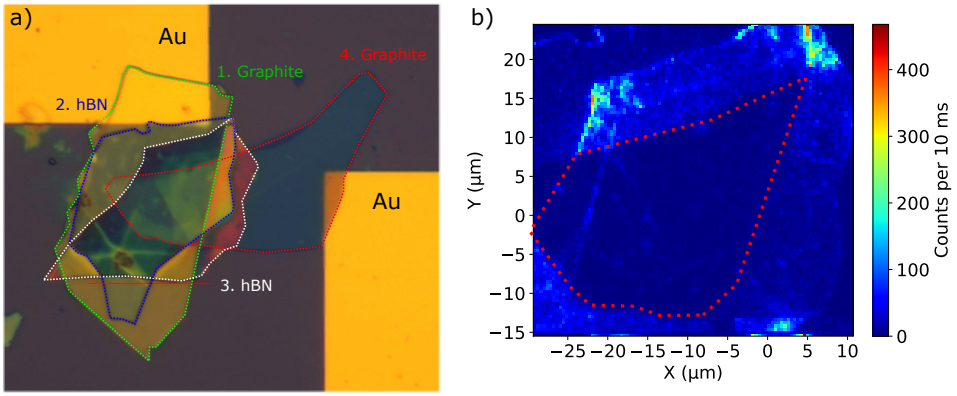

Figure 5.29.: Panel (a) shows a heterostructure with a thinner top graphite layer (see better contrast of overlap on the right electrode). Panel (b) shows the middle area of the heterostructure where all layers overlap. Some fluorescence signal is visible in the overlap region, bordered with the red dashed line.

One of the marked observations of terrylene on hBN is the existence of a very large inhomogeneous broadening, which also exists for molecule X. Compared to organic matrices, hBN can have significant tensile or shear strain in the layer, which can be present on nanometer scales.[76] Moreover, a report on the stretching of hBN has revealed that the emission wavelength of an emitter can be red-shifted up to tens of nm.[77] The experiment works by using an elastic substrate, such as PDMS, for the hBN, which can be stretched up to a few percent. Of course, the exact stretching of hBN itself is not known, as it depends on how well hBN conforms to the substrate. The notion that tensile strain, in this particular case, can strongly affect the emission wavelength, could be an appealing explanation for the large inhomogeneous broadening, i.e. large variations in the local environment of the molecule within diffraction-limited areas, that we observe for terrylene on hBN. We therefore propose a similar experiment that can test this hypothesis. For an optimal resolution of the spectra, this experiment could be best carried out at low temperature, using a piezo actuator to controllably exert strain and a structure that can amplify the expansion/contraction of the piezo. We have tried

a quick test at room temperature, by using hBN exfoliated onto PDMS. However, the large amount of Raman signal from the PDMS and the weak contrast of hBN flakes on PDMS (no interference effects giving colored flakes) made it difficult to observe the signal from single terrylene molecules.

5.7. CONCLUSION AND OUTLOOK

We have shown that terrylene molecules adsorbed on the surface of hBN become narrow emitters at low temperature, with linewidths as narrow as a few 100 MHz up to a few GHz. Their relative spectral stability, in contrast to single molecules adsorbed on any other surface so far, made it possible to observe 0-0 ZPLs on a surface. Moreover, we have found a way to considerably improve the spectral stability by annealing the hBN substrates before the molecules were deposited, which points to dynamics in the (organic) contamination as a potential source of the spectral jumps. Our work shows that narrow emission can also be observed for other molecules, if the right excitation wavelength is used. For example, the narrow emission from bulky graphene quantum dots was never observed before in other host matrices. This could indicate that hBN might be a host matrix for potentially many fluorescent molecules. This requires, however, more study on different types of molecules.

In future experiments, a well-known system such as terrylene could help shed light on the various issues of spectral instabilities and dephasing mechanisms, in order to improve the quality of other emitters hosted by hBN. For that reason, we propose two experiments that are based on experiments already conducted for the unknown emitters associated to hBN, to be repeated with terrylene molecules. The first experiment, which consists of applying large electric fields to the molecules, could potentially resolve the spectral diffusion and improve coherence properties of the molecules. In addition, if the action of two-level systems is completely suppressed by the large electric field, the strong linear broadening of the linewidth could be resolved as well, which may make narrow emission at higher-than-liquid-helium temperatures possible. The second experiment consists of the controlled application of strain on the hBN, to observe whether it would be possible to tune the molecule's resonance by strain. Moreover, it would be interesting to observe whether the molecular structure of terrylene can adapt to changes in the lattice parameters of hBN and whether this could be responsible for the reduced Franck-Condon factors that we observe for red-shifted molecules. In that way, the photon indistinguishability could perhaps be tuned and improved.

REFERENCES

(1) Cassabois, G.; Valvin, P.; Gil, B. *Nature Photonics* **2016**, *10*, 262–266.

(2) Gaudreau, L.; Tielrooij, K. J.; Prawiroatmodjo, G. E. D. K.; Osmond, J.; De Abajo, F. J. G.; Koppens, F. H. L. *Nano Letters* **2013**, *13*, 2030–2035.

(3) Han, S.; Qin, C.; Song, Y.; Dong, S.; Lei, Y.; Wang, S.; Su, X.; Wei, A.; Li, X.; Zhang, G.; Chen, R.; Hu, J.; Xiao, L.; Jia, S. *The Journal of Chemical Physics* **2021**, *155*, 244301.

(4) Hod, O. *Journal of Chemical Theory and Computation* **2012**, *8*, 1360–1369.

(5) Chen, T.-A.; Chuu, C.-P.; Tseng, C.-C.; Wen, C.-K.; Wong, H.-S. P.; Pan, S.; Li, R.; Chao, T.-A.; Chueh, W.-C.; Zhang, Y.; Fu, Q.; Yakobson, B. I.; Chang, W.-H.; Li, L.-J. *Nature* **2020**, *579*, 219–223.

(6) Maestre, C.; Toury, B.; Steyer, P.; Garnier, V.; Journet, C. *Journal of Physics: Materials* **2021**, *4*, 044018.

(7) Watanabe, K.; Taniguchi, T.; Kanda, H. *Nature Materials* **2004**, *3*, 404–409.

(8) Tran, T. T.; Bray, K.; Ford, M. J.; Toth, M.; Aharonovich, I. *Nature Nanotechnology* **2016**, *11*, 37–41.

(9) Bourrellier, R.; Meuret, S.; Tararan, A.; Stéphan, O.; Kociak, M.; Tizei, L. H. G.; Zobelli, A. *Nano Letters* **2016**, *16*, 4317–4321.

(10) Camphausen, R.; Marini, L.; Tawfik, S. A.; Tran, T. T.; Ford, M. J.; Palomba, S. *APL Photonics* **2020**, *5*, 076103.

(11) Gu, R.; Wang, L.; Zhu, H.; Han, S.; Bai, Y.; Zhang, X.; Li, B.; Qin, C.; Liu, J.; Guo, G.; Shan, X.; Xiong, G.; Gao, J.; He, C.; Han, Z.; Liu, X.; Zhao, F. *ACS Photonics* **2021**, *8*, 2912–2922.

(12) Li, X.; Shepard, G. D.; Cupo, A.; Camporeale, N.; Shayan, K.; Luo, Y.; Meunier, V.; Strauf, S. *ACS Nano* **2017**, *11*, 6652–6660.

(13) Aharonovich, I.; Tetienne, J.-P.; Toth, M. *Nano Letters* **2022**, *22*, 9227–9235.

(14) Dev, P. *Physical Review Research* **2020**, *2*, 022050.

(15) Neumann, M.; Wei, X.; Morales-Inostroza, L.; Song, S.; Lee, S.-G.; Watanabe, K.; Taniguchi, T.; Götzinger, S.; Lee, Y. H. *ACS Nano* **2023**, *17*, 11679–11691.

(16) Fleury, L.; Gruber, A.; Dräbenstedt, A.; Wrachtrup, J.; von Borczyskowski, C. *The Journal of Physical Chemistry B* **1997**, *101*, 7933–7938.

(17) Gmeiner, B.; Maser, A.; Utikal, T.; Götzinger, S.; Sandoghdar, V. *Physical Chemistry Chemical Physics* **2016**, *18*, 19588–19594.

(18) Vainer, Y. G.; Sobolev, Y. I.; Naumov, A. V.; Osad'ko, I. S.; Kador, L. *Faraday Discussions* **2015**, *184*, 237–249.

(19) Basché, T.; Bräuchle, C. *Chemical Physics Letters* **1991**, *181*, 179–186.

(20) Pazzagli, S.; Lombardi, P.; Martella, D.; Colautti, M.; Tiribilli, B.; Cataliotti, F. S.; Toninelli, C. *ACS Nano* **2018**, *12*, 4295–4303.

(21) Schofield, R. C.; Burdekin, P.; Fasoulakis, A.; Devanz, L.; Bogusz, D. P.; Hoggarth, R. A.; Major, K. D.; Clark, A. S. *ChemPhysChem* **2022**, *23*, e202100809.

(22) Faez, S.; van der Molen, S. J.; Orrit, M. *Physical Review B* **2014**, *90*, 205405.

(23) Türschmann, P.; Rotenberg, N.; Renger, J.; Harder, I.; Lohse, O.; Utikal, T.; Götzinger, S.; Sandoghdar, V. *Nano Letters* **2017**, *17*, 4941–4945.

(24) Shkarin, A.; Rattenbacher, D.; Renger, J.; Hönl, S.; Utikal, T.; Seidler, P.; Götzinger, S.; Sandoghdar, V. *Physical Review Letters* **2021**, *126*, 133602.

(25) Ren, P.; Wei, S.; Liu, W.; Lin, S.; Tian, Z.; Huang, T.; Tang, J.; Shi, Y.; Chen, X.-W. *Nature Communications* **2022**, *13*, 3982.

(26) Novoselov, K. S.; Geim, A. K.; Morozov, S. V.; Jiang, D.; Zhang, Y.; Dubonos, S. V.; Grigorieva, I. V.; Firsov, A. A. *Science* **2004**, *306*, 666–669.

(27) Anzai, Y.; Yamamoto, M.; Genchi, S.; Watanabe, K.; Taniguchi, T.; Ichikawa, S.; Fujiwara, Y.; Tanaka, H. *Applied Physics Express* **2019**, *12*, 055007.

(28) Haigh, S. J.; Gholinia, A.; Jalil, R.; Romani, S.; Britnell, L.; Elias, D. C.; Novoselov, K. S.; Ponomarenko, L. A.; Geim, A. K.; Gorbachev, R. *Nature Materials* **2012**, *11*, 764–767.

(29) Zhang, G.; Chang, Y.; Yan, B. *Crystals* **2023**, *13*, 304.

(30) Sonntag, J.; Li, J.; Plaud, A.; Loiseau, A.; Barjon, J.; Edgar, J. H.; Stampfer, C. *2D Materials* **2020**, *7*, 031009.

(31) Choi, S.; Tran, T. T.; Elbadawi, C.; Lobo, C.; Wang, X.; Juodkazis, S.; Seniutinas, G.; Toth, M.; Aharonovich, I. *ACS Applied Materials & Interfaces* **2016**, *8*, 29642–29648.

(32) Yim, D.; Yu, M.; Noh, G.; Lee, J.; Seo, H. *ACS Applied Materials & Interfaces* **2020**, *12*, 36362–36369.

(33) Gasparutti, I.; Song, S. H.; Neumann, M.; Wei, X.; Watanabe, K.; Taniguchi, T.; Lee, Y. H. *ACS Applied Materials & Interfaces* **2020**, *12*, 7701–7709.

(34) Navarro, P.; Tian, Y.; van Stee, M.; Orrit, M. *ChemPhysChem* **2014**, *15*, 3032–3039.

(35) Tchénio, P.; Myers, A. B.; Moerner, W. *Chemical Physics Letters* **1993**, *213*, 325–332.

(36) Kummer, S.; Kulzer, F.; Kettner, R.; Basché, T.; Tietz, C.; Glowatz, C.; Kryschi, C. *The Journal of Chemical Physics* **1997**, *107*, 7673–7684.

(37) Navarro, P.; Bocquet, F. C.; Deperasińska, I.; Pirug, G.; Tautz, F. S.; Orrit, M. *The Journal of Physical Chemistry C* **2015**, *119*, 277–283.

(38) Sontheimer, B.; Braun, M.; Nikolay, N.; Sadzak, N.; Aharonovich, I.; Benson, O. *Physical Review B* **2017**, *96*, 121202.

(39) White, S.; Stewart, C.; Solntsev, A. S.; Li, C.; Toth, M.; Kianinia, M.; Aharonovich, I. *Optica* **2021**, *8*, 1153.

(40) Vainer, Y. G.; Naumov, A. V.; Kol'chenko, M. A.; Personov, R. I. *physica status solidi (b)* **2004**, *241*, 3480–3486.

(41) Banasiewicz, M.; Wiącek, D.; Kozankiewicz, B. *Chemical Physics Letters* **2006**, *425*, 289–293.

(42) Nicolet, A. A. L.; Bordat, P.; Hofmann, C.; Kol'chenko, M. A.; Kozankiewicz, B.; Brown, R.; Orrit, M. *ChemPhysChem* **2007**, *8*, 1929–1936.

(43) Grandi, S.; Major, K. D.; Polisseni, C.; Boissier, S.; Clark, A. S.; Hinds, E. A. *Physical Review A* **2016**, *94*, 063839.

(44) Clear, C.; Schofield, R. C.; Major, K. D.; Iles-Smith, J.; Clark, A. S.; McCutcheon, D. P. S. *Physical Review Letters* **2020**, *124*, 153602.

(45) Tchénio, P.; Myers, A. B.; Moerner, W. *Journal of Luminescence* **1993**, *56*, 1–14.

(46) Li, C.; Xu, Z.-Q.; Mendelson, N.; Kianinia, M.; Toth, M.; Aharonovich, I. *Nanophotonics* **2019**, *8*, 2049–2055.

(47) Zobelli, A.; Ewels, C. P.; Gloter, A.; Seifert, G. *Physical Review B* **2007**, *75*, 094104.

(48) Chen, X.; Sun, H.; Zhang, W.; Tan, C.; Liu, X.; Zhao, J.; Hou, L.; Gao, Y.; Song, J.; Chen, Z. *Vacuum* **2022**, *199*, 110935.

(49) Arnold, T.; Forster, M.; Fragkoulis, A. A.; Parker, J. E. Structure of Normal-Alkanes Adsorbed on Hexagonal-Boron Nitride, EN, research-article, 2014.

(50) Glushkov, E.; Macha, M.; Räth, E.; Navikas, V.; Ronceray, N.; Cheon, C. Y.; Ahmed, A.; Avsar, A.; Watanabe, K.; Taniguchi, T.; Shorubalko, I.; Kis, A.; Fantner, G.; Radenovic, A. *ACS Nano* **2022**, *16*, 3695–3703.

(51) Xu, Z.-Q.; Elbadawi, C.; Tran, T. T.; Kianinia, M.; Li, X.; Liu, D.; Hoffman, T. B.; Nguyen, M.; Kim, S.; Edgar, J. H.; Wu, X.; Song, L.; Ali, S.; Ford, M.; Toth, M.; Aharonovich, I. *Nanoscale* **2018**, *10*, 7957–7965.

(52) Noé, J. C.; Nutz, M.; Reschauer, J.; Morell, N.; Tsioutsios, I.; Reserbat-Plantey, A.; Watanabe, K.; Taniguchi, T.; Bachtold, A.; Högele, A. *Nano Letters* **2018**, *18*, 4136–4140.

(53) Lawetz, V.; Orlandi, G.; Siebrand, W. *The Journal of Chemical Physics* **1972**, *56*, 4058–4072.

(54) Kummer, S.; Basché, T.; Bräuchle, C. *Chemical Physics Letters* **1994**, *229*, 309–316.

(55) Basché, T.; Kummer, S.; Bräuchle, C. *Nature* **1995**, *373*, 132–134.

(56) Banasiewicz, M.; Morawski, O.; Wiącek, D.; Kozankiewicz, B. *Chemical Physics Letters* **2005**, *414*, 374–377.

(57) Nicolet, A.; Kol'chenko, M. A.; Kozankiewicz, B.; Orrit, M. *The Journal of Chemical Physics* **2006**, *124*, 164711.

(58) Fleury, L.; Tamarat, P.; Kozankiewicz, B.; Orrit, M.; Lapouyade, R.; Bernard, J. *Molecular Crystals and Liquid Crystals* **1996**, *283*, 81–87.

(59) Neumann, A.; Lindlau, J.; Thoms, S.; Basché, T.; Högele, A. *Nano Letters* **2019**, *19*, 3207–3213.

(60) Trinh, C. T.; Lee, J.; Lee, K.-G. *Scientific Reports* **2018**, *8*, 8273.

(61) Ronceray, N.; You, Y.; Glushkov, E.; Lihter, M.; Rehl, B.; Chen, T.-H.; Nam, G.-H.; Borza, F.; Watanabe, K.; Taniguchi, T.; Roke, S.; Keerthi, A.; Comtet, J.; Radha, B.; Radenovic, A. *Nature Materials* **2023**, *22*, 1236–1242.

(62) Lavie, J.; Vu, V. B.; Medina-Lopez, D.; Dappe, Y.; Liu, T.; Rondin, L.; Lauret, J.-S.; Latil, S.; Campidelli, S. *Helvetica Chimica Acta* **2023**, *106*, e202300034.

(63) Levy-Falk, H.; Capelle, O.; Liu, T.; Medina-Lopez, D.; Deleporte, E.; Campidelli, S.; Rondin, L.; Lauret, J.-S. *physica status solidi (b)* **2023**, *260*, 2300310.

(64) Medina-Lopez, D.; Liu, T.; Osella, S.; Levy-Falk, H.; Rolland, N.; Elias, C.; Huber, G.; Ticku, P.; Rondin, L.; Jousselme, B.; Beljonne, D.; Lauret, J.-S.; Campidelli, S. *Nature Communications* **2023**, *14*, 4728.

(65) Liu, T.; Carles, B.; Elias, C.; Tonnelé, C.; Medina-Lopez, D.; Narita, A.; Chassagneux, Y.; Voisin, C.; Beljonne, D.; Campidelli, S.; Rondin, L.; Lauret, J.-S. *The Journal of Chemical Physics* **2022**, *156*, 104302.

(66) Ajayi, O. A.; Ardelean, J. V.; Shepard, G. D.; Wang, J.; Antony, A.; Taniguchi, T.; Watanabe, K.; Heinz, T. F.; Strauf, S.; Zhu, X.-Y.; Hone, J. C. *2D Materials* **2017**, *4*, 031011.

(67) Wierzbowski, J.; Klein, J.; Sigger, F.; Straubinger, C.; Kremser, M.; Taniguchi, T.; Watanabe, K.; Wurstbauer, U.; Holleitner, A. W.; Kaniber, M.; Müller, K.; Finley, J. J. *Scientific Reports* **2017**, *7*, 12383.

(68) Zhang, X.; Xu, C.; Zou, Z.; Wu, Z.; Yin, S.; Zhang, Z.; Liu, J.; Xia, Y.; Lin, C.-T.; Zhao, P.; Wang, H. *Carbon* **2020**, *161*, 479–485.

(69) Allard, C.; Schué, L.; Fossard, F.; Recher, G.; Nascimento, R.; Flahaut, E.; Loiseau, A.; Desjardins, P.; Martel, R.; Gaufrès, E. *Advanced Materials* **2020**, *32*, 2001429.

(70) Tran, T. T.; Kianinia, M.; Nguyen, M.; Kim, S.; Xu, Z.-Q.; Kubanek, A.; Toth, M.; Aharonovich, I. *ACS Photonics* **2018**, *5*, 295–300.

(71) Konthasinghe, K.; Chakraborty, C.; Mathur, N.; Qiu, L.; Mukherjee, A.; Fuchs, G. D.; Vamivakas, A. N. *Optica* **2019**, *6*, 542.

(72) Ngoc My Duong, H.; Nguyen, M. A. P.; Kianinia, M.; Ohshima, T.; Abe, H.; Watanabe, K.; Taniguchi, T.; Edgar, J. H.; Aharonovich, I.; Toth, M. *ACS Applied Materials & Interfaces* **2018**, *10*, 24886–24891.

(73) Fournier, C.; Plaud, A.; Roux, S.; Pierret, A.; Rosticher, M.; Watanabe, K.; Taniguchi, T.; Buil, S.; Quélin, X.; Barjon, J.; Hermier, J.-P.; Delteil, A. *Nature Communications* **2021**, *12*, 3779.

(74) Akbari, H.; Biswas, S.; Jha, P. K.; Wong, J.; Vest, B.; Atwater, H. A. *Nano Letters* **2022**, *22*, 7798–7803.

(75) Somaschi, N.; Giesz, V.; De Santis, L.; Loredo, J. C.; Almeida, M. P.; Hornecker, G.; Portalupi, S. L.; Grange, T.; Antón, C.; Demory, J.; Gómez, C.; Sagnes, I.; Lanzillotti-Kimura, N. D.; Lemaítre, A.; Auffeves, A.; White, A. G.; Lanco, L.; Senellart, P. *Nature Photonics* **2016**, *10*, 340–345.

(76) Hayee, F.; Yu, L.; Zhang, J. L.; Ciccarino, C. J.; Nguyen, M.; Marshall, A. F.; Aharonovich, I.; Vučković, J.; Narang, P.; Heinz, T. F.; Dionne, J. A. *Nature Materials* **2020**, *19*, 534–539.

(77) Mendelson, N.; Doherty, M.; Toth, M.; Aharonovich, I.; Tran, T. T. *Advanced Materials* **2020**, *32*, 1908316.